dCas9-based *Scn1a* gene activation restores inhibitory interneuron excitability and attenuates seizures in Dravet syndrome mice

Gaia Colasante[1#*], Gabriele Lignani[2#], Simone Brusco[1], Claudia Di Berardino[1], Jenna Carpenter[2], Serena Giannelli[1], Nicholas Valassina[1], Simone Bido[1], Raffaele Ricci[1], Valerio Castoldi[3], Silvia Marenna[3], Timothy Church[2], Luca Massimino[1], Giuseppe Morabito[1], Fabio Benfenati[4,5], Stephanie Schorge[2], Letizia Leocani[3], Dimitri M. Kullmann[2] and Vania Broccoli[1,6,*]

[1]Stem Cell and Neurogenesis Unit, Division of Neuroscience, San Raffaele Scientific Institute, 20132 Milan, Italy; [2]Department of Clinical and Experimental Epilepsy, UCL Institute of Neurology, University College London, Queen Square, London, WC1N 3BG, UK; [3]Experimental Neurophysiology Unit, Institute of Experimental Neurology (INSPE), San RaffaeleScientific Institute, 20132 Milan Italy; [4]Center for Synaptic Neuroscience and Technology, Istituto Italiano di Tecnologia, 16132 Genova, Italy; [5]IRCCS Ospedale Policlinico San Martino, University of Genova, 16132 Genova, Italy. [6]CNR Institute of Neuroscience, 20129 Milan, Italy.

#These authors share first authorship

*Corresponding authors

Correspondence should be addressed to:

Vania Broccoli - Stem Cells and Neurogenesis Unit, Division of Neuroscience, San Raffaele Scientific Institute, Via Olgettina 58, 20132 Milan, Italy. Tel: +39 02 26434616; FAX +39 02 26436585. E-mail: broccoli.vania@hsr.it. Website: www.vaniabroccolilab.com.

Or to:

Gaia Colasante - Stem Cells and Neurogenesis Unit, Division of Neuroscience, San Raffaele Scientific Institute, Via Olgettina 58, 20132 Milan, Italy. Tel: +39 02 26435790.

E-mail: colasante.gaia@hsr.it

Short title: dCas9-based *Scn1a* gene activation in Dravet syndrome

Abstract

Dravet syndrome (DS) is a severe epileptic encephalopathy caused mainly by heterozygous loss-of-function mutations of the *SCN1A* gene, indicating haploinsufficiency as the pathogenic mechanism. Here, we tested whether catalytically dead Cas9 (dCas9)-mediated *Scn1a* gene activation can rescue *Scn1a* haploinsufficiency in a mouse DS model and restore physiological levels of its gene product, the $Na_v1.1$ voltage-gated sodium channel. We screened single guide RNAs (sgRNAs) for their ability to stimulate *Scn1a* transcription in association with the dCas9 activation system. We identified a specific sgRNA that increases *Scn1a* gene expression levels in cell lines and primary neurons with high specificity. $Na_v1.1$ protein levels were augmented, as was the ability of wild-type immature GABAergic interneurons to fire action potentials. A similar enhancement of *Scn1a* transcription was achieved in mature DS interneurons, thus rescuing their ability to fire. To test the therapeutic potential of this approach, we delivered the *Scn1a*-dCas9 activation system to DS pups using adeno-associated viruses. Parvalbumin interneurons recover their firing ability and febrile seizures were significantly attenuated. Our results pave the way for exploiting dCas9-based gene activation as an effective and targeted approach in DS and other disorders resulting from altered gene dosage.

Introduction

Dravet syndrome (DS) is a severe epileptic encephalopathy beginning in the first year of life with seizures often associated with fever that subsequently evolve into frequent, prolonged and clustered epileptic crises [1–3]. In the subsequent years, patients often develop psychomotor delay, behavioral disturbances and cognitive impairment[4]. DS is a genetic condition mainly caused by mutations in the *SCN1A* gene encoding for the $Na_v1.1$ voltage-gated sodium channel alpha-subunit[5,6]. Over 650 missense and nonsense *SCN1A* mutations have been described in DS patients. Although most are de novo, some mutations have been found to be inherited in familial cases[7]. *SCN1A* mutations affect only one copy of the gene typically leading to loss-of-function and indicating that a haploinsufficient genetic mechanism is responsible for DS. These data suggest that a reduced amount of $Na_v1.1$ channel impairs neuronal activity and function. *Scn1a* heterozygous mutant mice display similar neurological symptoms including severe epilepsy, behavioral alterations and premature death[8–11]. Functional studies revealed that cortical fast-spiking GABAergic inhibitory interneurons exhibited a reduced intrinsic excitability and defects in action potential firing[8,10,12]. In contrast, both excitability and firing of cortical excitatory neurons from *Scn1a* heterozygous mutant mice appeared substantially unaltered[8,13]. These findings potentially resolve the paradox that epilepsy arises from loss-of-function mutations in $Na_v1.1$, which contributes to the fast depolarization of neuronal membranes during an action potential. Of note, $Na_v1.1$ was found to be mainly expressed in inhibitory interneurons by immunohistochemistry analysis suggesting that this sodium channel isoform has a preponderant function in that neuronal population[10]. Accordingly, selective inactivation of *Scn1a* in cortical interneurons is sufficient to elicit neurological deficits comparable to those described in constitutive mutant mice[14,15], and conversely *Scn1a* loss restricted to the dorsal-telencephalic (e.g. neocortical, hippocampal) excitatory neurons has ameliorating effects for epileptic seizures and sudden death[13]. *Scn1a* heterozygous mutant mice develop spontaneous and recurrent seizures starting from 3 weeks after birth often leading to premature and sudden death[8–10]. Remarkably, body temperature elevation triggers myoclonic and generalized seizures in these mice recapitulating febrile seizures in DS patients[16]. Thus, DS mice represent a valuable model of the disease, not only to dissect the pathological mechanisms but also to evaluate the efficacy of innovative therapies. Drug treatment of DS patients, including stiripentol in combination with clobazam and valproate, has limited efficacy and poorly controls convulsive seizures[17,18]. Cannabidiol or serotonin- uptake inhibitors have been reported to reduce seizure frequency in some patients but larger studies are needed to appreciate the exact therapeutic indications for these treatments[19–21]. Nonetheless, complete seizure cessation is rarely obtained with any of these pharmacological anticonvulsants. Gene therapy approaches for neurodevelopmental disorders are

in rapid development thanks to the introduction of novel serotypes of recombinant adeno-associated viruses (AAVs) allowing efficient transduction of neurons[22]. However, the *Scn1a* coding sequence is 6 kb long, exceeding the strict cargo limit for AAVs. Although lentiviruses can carry the *Scn1a* gene sequence, they show limited spread in neural tissue, and are therefore inadequate to treat diseases affecting large brain areas[23]. These obstacles have prevented substantial advances in gene-based therapies for DS. Given that, one copy of the *SCN1A* gene is still functional in DS, stimulating its endogenous expression over physiological levels might lead to an increasing availability of the $Na_v1.1$ channel protein, potentially leading to symptomatic improvement. Thus, a system able to induce *SCN1A* gene expression in neurons in a regulated manner, without significant off-target effects, would be a strong therapeutic candidate tool for DS.

The CRISPR-Cas9 (Clustered Regularly Interspaced Short Palindromic Repeats-CRISPR associated protein 9) technology has become a powerful tool for genome editing, allowing DNA to be targeted with high efficiency and specificity. As demonstrated by pioneering works in several cell types and organisms, the Cas9/sgRNA complex can efficiently generate double strand breaks, which then trigger non-homologous end-joining-mediated gene knockout or homology-directed repair-mediated recombination[24–26]. A modified version of the CRISPR-Cas9 system has been developed by generating a nuclease-dead Cas9 (dCas9) fused to effector domains for transcriptional gene regulation. Hence, the dCas9/sgRNA complex has provided a crucial platform for programming diverse types of transcriptional or epigenetic manipulation of the genome without cleaving the target DNA[27–29]. Seminal studies have shown that dCas9-based gene activation is highly specific in DNA-binding and gene regulation and promotes chromatin remodeling of the regulatory elements of the gene of interest[30–32]. This system has been successfully implemented to investigate hierarchies in gene regulatory networks, screening for cellular phenotypes and directing somatic cell fate[33–36]. In the activatory CRISPR system the dCas9 has been fused to multiple VP16 transcriptional activation that robustly activates gene transcription when combined with one or more sgRNAs targeting sequences in the proximal promoters or close to transcription start sites (TSSs)[26,36,37]. As proof-of concept, this technology has also been employed to activate endogenous genes in mouse models of diseases to ameliorate biomarkers of diabetes, muscular dystrophy and acute kidney disease[30]. More recently it has been applied to enhance the expression of Sim1 gene in the hypothalamus and to rescue the associated obesity phenotype[38]. Here we describe a dCas9-based system to significantly up-regulate *Scn1a* expression and to restore $Na_v1.1$ protein levels in both cellular and animal models of DS. This targeted gene activation rescues membrane excitability and action potential firing in DS cortical interneurons and significantly attenuates hyperthermia-induced seizures in DS mice.

Results

A single sgRNA enhances *Scn1a* gene expression by targeting its proximal promoter

To achieve upregulation of *Scn1a* gene transcription, we sought to define the necessary dCas9/sgRNA elements by a candidate approach *in vitro*. Through an extensive bioinformatics analysis, we determined the *Scn1a* gene promoter regions to focus the sgRNA design. Several studies have pointed out that sgRNAs can transactivate genes of interest more efficiently if localized within the 500 base pairs (bp) from the gene TSS[34] . We interrogated the ENCODE and Fantom5 databases for the expression profiling and epigenetic marks of actively transcribed genes in the adult mouse brain. In addition, CAGE-seq and DNase-seq datasets were queried to determine the exact TSSs for *Scn1a* (**Figure S1**). We identified two regions in the *Scn1a* locus where RNA PolII, mono- and tri-methylation of lys4 and acetylation of lys27 of H3 histone were strongly enriched and that revealed DNAse I hypersensitive sites. CAGE-seq peaks were aligned to the same sequences, confirming the existence of two active TSSs (TSS1 and TSS2) located upstream to two non-coding exons (Exon-A and Exon-B) (**Figure S1**) and producing two different mRNA isoforms, both expressed in the adult mouse brain[39]. 200 bps upstream to the exon-A (distal promoter) and 250 bps upstream to exon-B (proximal promoter) (**Figure 1A**) were submitted to the *CRISPOR* web tool (*http://crispor.tefor.net*) for sgRNA design. We selected five guides in the distal promoter and six in the proximal one, with specificity scores higher than 50% (**Figures 1B, C; Supplementary Table 1**). Then, we determined if dCas9 fused to VP160 (dCas9-VP160), a transcriptional activator that carries 10 tandem copies of VP16 (a herpes simplex virus type 1 transcription factor), in association with the selected sgRNAs was able to upregulate *Scn1a* gene expression in the P19 murine teratocarcinoma cell line. sgRNAs specific for *Scn1a* promoters and one control guide (sgCtrl), targeting the beta-galactosidase bacterial sequence, were cloned into the pU6 vector and individually lipofected into P19 cells together with the Ef1a-dCas9-VP160-T2A-GFP (**Figure 1D**) and 3 days later, after ascertaining GFP expression, cells were harvested for RNA extraction and RT-qPCR (**Figure 1D**). Interestingly, none of the sgRNAs targeting the distal promoter were able to significantly alter the basal expression of *Scn1a* (**Figure 1E**). Conversely, among the guides targeting the proximal promoter, only sg1P was found to significantly increase *Scn1a* mRNA levels with respect to sgCtrl (**Figure 1F**). Comparable results were obtained when sgRNAs were lipofected with a dCas9 linked to a puromycine resistance cassette (Ef1a-dCas9-VP160-T2A-Puro^{R}) and puromycine was added to the culture medium the day after the trasfection (**Figures S2A-C**), indicating that antibiotic selection and consequent enrichment of lipofected cells was not strictly necessary to detect the sg1P-mediated *Scn1a* induction. sg1P upregulated *Scn1a* gene expression to

a similar extent in primary mouse embryonic fibroblasts (MEFs) (**Figure S2D**). In conclusion, we identified sg1P as an sgRNA that is sufficient, when associated with the dCas9 activation system, to stimulate basal transcription of *Scn1a* consistently in different cell types.

sg1P/dCas9-VP160 lentiviral transduction upregulates *Scn1a* expression in primary neurons

We asked whether the sg1P/dCas9-VP160 system could stimulate *Scn1a* expression in primary hippocampal neurons. Neurons were co-transduced with Ef1a-dCas9VP160-T2A-GFP and pU6-sg1P or pU6-sgCtrl lentiviruses the day after plating to maximize transduction efficiency (**Figure 2A**). Immunofluorescence analysis performed at 10 DIV showed that almost 50% of the plated neurons were transduced (**Figure 2B**). With this intermediate efficiency, we decided to purify the infected cells in order to obtain reliable information on the regulation of *Scn1a* expression. Thus, 10 DIV transduced GFP^+ neurons from sgCtrl and sg1P-treated samples were isolated by fluorescence activated cell sorting (FACS) (**Figure 2C**) and the RNA was extracted for gene expression analysis. *Scn1a* expression levels were robustly increased when transduced with sg1P with respect to sgCtrl (**Figure 2D**). However, FACS is detrimental to neurons and prevents their functional analysis. For this reason, we generated a single lentiviral vector carrying both the sg1P and dCas9-VP160 (**Figure 2E**), which improved transduction efficiency up to ~75% (**Figure 2F**). In this setting a 4-fold increase in *Scn1a* expression was detected in sg1P with respect to sgCtrl treated neurons. Moreover, no alteration in the transcriptional levels of the second *Scn1a* mRNA isoform carrying exon-A was detectable (**Figure 2G**), indicating that the sg1P/dCas9-VP160 activation system does not impact the transcriptional status of the distal promoter. To evaluate whether increased transcription of *Scn1a* led to higher $Na_v1.1$ protein levels, we performed Western blot analysis of membrane lysates isolated from transduced 10 DIV primary neuronal cultures, which showed a two-fold increase in membrane-associated $Na_v1.1$ protein (**Figure 2H**).

Taken together, these results indicate that sg1P associated with the dCas9 activation system can modulate *Scn1a* gene activity in primary neurons and accordingly increase the levels of the $Na_v1.1$ channel protein.

dCas9-based gene activation is highly specific for Scn1a in primary neurons

We examined the specificity of the dCas9 activation system by assessing global gene expression in primary neurons transduced with dCas9-VP160 together with either sg1P or sgCtrl. RNA-seq was performed on 3 DIV neurons, 2 days after lentiviral transduction with either sg1P or the control guide (**Figure 3A**). Notably, the only gene with significantly increased expression relative to control was *Scn1a* (log2 fold change > 1.5, $p < 0.005$), indicating the high specificity of the dCas9 activation

system in primary neuronal cells (**Figures 3B, red dots**). CRISPOR provided a list of 195 putative off-target genes associated with the sg1P. As dCas9A is nuclease defective, we reasoned that aspecific transcription activation could occur only if off-target sequences were in close proximity to TSSs of genes. Therefore, we filtered the list by the web tool Galaxy to investigate which of those putative off-targets were located within 500 base pairs of TSSs of any annotated gene. Only 4 out of 195 putative off-target genes were identified in the putative promoter regions upstream to the Prp4, BC02, Olfr919 and Plrg1 genes. However, from both sequencing and qRT-PCR analyses, the expression of these genes was not altered after delivery of the dCas9 activation system (**Figures 3B, C *left panel yellow dots***).

Absolute and relative levels of the various Na_v alpha-subunits are strictly regulated, allowing fine balance of neuronal membrane excitability[40]. Therefore, we examined the expression of other Na_v alpha-subunit encoding genes. The global transcriptional analysis revealed no significant change in their expression levels (**Figure 3B, *right panel yellow dots***). These results were confirmed by RT-qPCR assays on independent cellular replicates (**Figur 3C, *right panel***). In conclusion, both the global and targeted gene expression analysis on primary neurons transduced with the sg1P-dCas9 activation system (henceforward *Scn1a*-dCas9A) confirmed the high specificity for *Scn1a* gene transactivation at genome-wide level.

dCas9-based *Scn1a* gene activation enhances neuronal activity in immature wild-type cortical interneurons

To evaluate whether the increased levels of $Na_v1.1$ protein in primary neurons was sufficient to alter neuronal excitability, whole-cell path clamp experiments were carried out in dCas9A-transduced neurons. We conceived a dual lentiviral inducible system designed with a first lentivector carrying the dCas9-VP160 with tdTomato reporter regulated by rtTA responsive element (TRE) and a second lentivector carrying the transactivator rtTA and sgRNAs (sg1P or sgCtrl), to explore a setting that will reveal relevant in *in vivo* experiments (**Figure 4A** and **Figure S3A**). Indeed, the split of *Scn1a*-dCas9A in two vectors is required for the *in vivo* delivery mediated by adeno-associated vectors (AAVs), characterized by a limited cargo capacity. In this setting, upon doxycycline (dox) administration, about 60% of neurons were transduced (**Figure S3B**). A 2-fold increase of the basal level of Scn1a gene expression (Scn1a-dCas9A vs Ctrl- dCas9A) in wt neurons at 7 DIV was observed upon dox administration (**Figure S3C**, +dox), but not in dox absent condition (-dox), although some leaky expression of dCas9A could be detected (**Figure S3D**).

Since $Na_v1.1$ channel loss mainly affects GABAergic interneurons, we established primary neuronal cultures from GAD67-GFP mouse embryos that were transduced with either the Ctrl-

dCas9A or *Scn1a*-dCas9A system and analyzed when double positive for GFP and tdTomato (**Figures 4A,B**).

First recordings were performed on 9-11 DIV primary neurons, before their achievement of full functional maturation. Current step injections showed a significant increase in firing rate in interneurons transduced with *Scn1a*- compared to Ctrl-dCas9 activation system (Ctrl-dCas9A n=11; *Scn1a*-dCas9A n=15; p=0.03 Mann-Whitney non-parametric *t*-test) (**Figures 4C-E**; **Figure S4**). No alteration of neuronal firing rate was mediated by *Scn1a*-dCas9A in the absence of dox (**Figure S3E).** These results underline the potential efficiency of the *Scn1a*-dCas9A to increase interneuron excitability upon alteration of *Scn1a* gene dosage, at least in an immature network.

Recently, we developed a new electrophysiological approach ('activity clamp') to analyze how a neuron in a given epileptic network responds to antiepileptic drugs[41]. Here, we modified this method to adapt it for primary neuronal cultures in order to compare interneurons transduced with either the Ctrl-dCas9A or *Scn1a*-dCas9A system. First, we recorded in interneurons the barrage of AMPA receptor-mediated excitatory synaptic currents that occurs in the presence of the chemoconvulsant potassium channel blocker 4-Aminopyridine (4-AP). Then, we converted the recorded currents into a conductance waveform, and by applying dynamic current clamp we fed them back to interneurons pharmacologically isolated from the network. We then compared neurons transduced with either the *Scn1a*- or the Ctrl-dCas9A system (**Figures 4F-I**). Activity clamp showed that GABAergic interneurons transduced with *Scn1a*-dCas9A exhibited an increase in the number of action potentials (APs) evoked by the same epileptic inputs, as well as higher firing frequencies reached during the protocol (Ctrl-dCas9A n = 10; *Scn1a*-dCas9A n = 12; p = 0.0009, Parametric Student`s *t*-test) (**Figure 4I**). Altogether, these results indicate that increased expression of *Scn1a* obtained by the dCas9A system is sufficient to increase interneuron excitability in response to epileptiform barrages of synaptic excitation.

dCas9-based *Scn1a* activation increases $Na_v1.1$ protein levels and rescues excitability in *Scn1a*$^{+/-}$ mutant cortical interneurons

The experiments described above show that the *Scn1a*-dCas9A system up-regulates *Scn1a* expression in wild-type interneurons, increasing $Na_v1.1$ protein levels, and enhance their excitability. We asked whether this system could also boost the transcription of the single wild-type *Scn1a* allele in DS mice, to reach sufficient $N_{av}1.1$ protein levels to compensate haploinsufficiency and attenuate the pathology.

We tested the efficacy of the *Scn1a*-dCas9A system in *Scn1a*$^{+/-}$ neurons derived from a DS mouse model [10] (**Figure 5A**). Considering that *Scn1a* gene starts to be expressed postnatally around

P10[10,42], the analysis was done at DIV 22-25 to ensure the display of characteristic DS phenotype to DS. Interestingly, at this time point, wild-type neurons seem to be unresponsive to *Scn1a*-dCas9A treatment (**Figure 5B**), while we observed a 3.5-fold increase in levels of *Scn1a* expression in *Scn1a*-dCas9A- compared to Ctrl-dCas9A-treated DS neurons (**Figure 5C**). To assess the nature of Scn1a-dCas9A induced mRNA, we performed deep sequencing of PCR amplicons spanning the mutation region and found out that in Ctrl-dCas9A transduced neurons corresponding to basal conditions, wild-type and mutant transcripts were approximately equally abundant (almost 50% each) (**Figure 5D**). The same relative proportion was maintained in Scn1a-dCas9A-treated neurons (**Figure 5D**). These data indicate that mutant mRNA is stable in DS neurons and consequently that Scn1a-dCas9A treatment induces up-regulation of both transcripts. However, at the protein level, untreated *Scn1a*$^{+/-}$ postnatal brains showed a ~50% reduction of $Na_v1.1$ protein levels with respect to the control counterparts (**Figures 5E,F).** In accordance with mRNA data, levels of Nav1.1 protein do not change upon *Scn1a*-dCas9A in *Scn1a*+/+ neurons while, remarkably, *Scn1a*-dCas9A treated *Scn1a*$^{+/-}$ neurons exhibited almost doubled $Na_v1.1$ protein levels compared to Ctrl-dCas9A treated *Scn1a*$^{+/-}$ neurons at 25 DIV (**Figures 5E,F**). Immunoblot signal lower than 170 kDa and corresponding to truncated $Na_v1.1$ protein was not observed either in *Scn1a*$^{+/-}$ adult brains or in *Scn1a*$^{+/-}$ neurons under basal conditions (Ctrl-dCas9A) or treated with Scn1a-dCas9A (**Figures 5E).** These results imply that the mutant protein is likely degraded and not targeted to the plasma membrane. To assess whether the rescue of $Na_v1.1$ protein levels has a functional impact on DS neurons, electrophysiological experiments were repeated in *Scn1a*$^{+/-}$;GAD67-GFP GABAergic interneurons transduced either with the Ctrl-dCas9A or *Scn1a*-dCas9A system (**Figures 6A,B**). Recordings were performed on 18-20 DIV neuronal cultures in order to treat fully mature and functional interneurons. Current step injections showed a decreased frequency-current relationship and maximum AP frequency in *Scn1a*$^{+/-}$ interneurons compared to wild type, when both were transduced with the Ctrl-dCas9A system (**Figures 6C,D,E**). Accordingly, an increased current threshold to trigger a single AP was observed (**Figure 6G**). These defects in *Scn1a*$^{+/-}$ interneurons were completely rescued by transducing the Scn1a-dCas9A system (Ctrl wild-type n = 12; Ctrl *Scn1a*$^{+/-}$ n = 10; Scn1a-dCas9A wild-type n = 10; *Scn1a*-dCas9A *Scn1a*$^{+/-}$ n = 11. p = 0.02; p = 0.04, 2-way ANOVA followed by the Bonferroni's multiple comparison test) (**Figures 6D-H**). Activity clamp confirmed a rescue of DS mutant interneuron firing in the face of epileptiform activity following *Scn1a*-dCas9A treatment compared to the Ctrl-dCas9A treatment (Ctrl-dCas9A wild-type n = 12; Ctrl-dCas9A *Scn1a*$^{+/-}$ n = 10; *Scn1a*-dCas9A wild-type n = 10; *Scn1a*-dCas9A *Scn1a*$^{+/-}$ n = 11. p = 0.03, 2-way ANOVA followed by the Bonferroni's multiple comparison test) (**Figure**

6I). As expected by molecular data, the increase in excitability in *Scn1a*-dCas9A treated wild-type interneurons observed at 9-10 DIV was no longer observed at 18-20 DIV (**Figures 6C-J**).

AAV-mediated *Scn1a*-dCas9A transduction of cortical interneurons rescues PV+ interneuron deficiency and protects *Scn1a*$^{+/-}$ mutant mice from hyperthermia-induced seizures

Given the encouraging results with the *Scn1a*-dCas9A treatment obtained on neuronal cultures, we sought to test its efficacy in rescuing the epileptic phenotype in a DS mouse model.

To exploit the *Scn1*a-dCas9A system *in vivo,* we sought to stimulate *Scn1a* expression selectively in forebrain GABAergic interneurons. Therefore, we used a dual AAV9 based system as these viral particles diffuse efficiently in the brain parenchyma after intracerebroventricular (ICV) injections in neonatal mouse pups[43]. The VP64 activator domain, carrying four tandem copies of VP16, was chosen for the *in vivo* delivery as its smaller size allows this dCas9A together with the TRE promoter to fit in an AAV vector. Similarly to aforementioned dual lentiviral system, a second AAV9 was packaged with the sg1P cassette followed by the mDlx5/6 promoter driving selective expression of the rtTA-T2A-Tomato cassette in forebrain GABAergic interneurons (**Figure 7A**)[44,45].

When the mDlx5/6-promoter driven dCas9A elements were virally transduced in GAD67-GFP transgenic pups, we estimated that about 85% of the viral reporter tdTomato^{+} cells in the cerebral cortex also expressed the GFP transgene (**Figures S7A-C,F**). Furthermore, different interneuron subtypes could be targeted specifically by our system as shown by co-labeling of tdTomato with either Parvalbumin, Somatostatin, NPY or VIP (**Figures S6B-F**). Histological characterization of wild-type litters injected with the dCas9A elements revealed discrete transduction efficiency along the antero-posterior axis, with about 20% of total GABAergic interneurons transduced in cortical areas close to injection sites (Cx1_L, left and Cx1_R, right) (**Figure S6G**). Neatly, in these same areas, a significant increase in *Scn1a* gene expression was detected in 2 week-old mice treated with the *Scn1a*- dCas9A system compared to the Ctrl-dCas9A system (**Figures 7B,C)**. To assess if *Scn1a*- dCas9A has a functional effect on PV interneurons in vivo, we performed patch-clamp analysis on treated *Scn1a*$^{+/+}$ and *Scn1a*$^{+/-}$ mice crossed with PV-Cre;Ai9-tdTomato mice at P21-P28 (**Figure S7A**).

Current step injections highlighted a decreased frequency-current relationship (**Figure S7C)** and maximum AP frequency (**Figure S7D)** in *Scn1a*$^{+/-}$ PV interneurons compared to *Scn1a*$^{+/+}$, when injected with Ctrl-dCas9A. These defects in *Scn1a*$^{+/-}$ PV interneurons were rescued by transducing the Scn1a-dCas9A system (*Scn1a*$^{+/+}$*;* Ctrl-dCas9A n=9; *Scn1a*$^{+/-}$;Ctrl-dCas9A n=12; *Scn1a*$^{+/-}$*;Scn1a*-dCas9A n=11; I/O: p=0.003, two-way ANOVA (**Figures S7C,D**).

At one month, *Scn1a*$^{+/-}$ mice were implanted with electrodes and EEG was recorded after subjecting the mice to hyperthermia-induced seizures. When *Scn1a*$^{+/-}$ mice were exposed to hyperthermia, we observed that the seizure threshold temperature was increased in *Scn1a*-dCas9A- compared to Ctrl-dCas9A-treated mice (Ctrl-dCas9A: 41.93 ± 0.1687, n=6; *Scn1a*-dCas9A: 42.343 ± 0.1453, n=6; p=0.0048, Student's *t* test) (**Figure 7F**). Furthermore, *Scn1a*-dCas9A-treated *Scn1a*$^{+/-}$ mice displayed seizures with a generally lower average clinical severity score than Ctrl-dCas9A-treated mice (Ctrl-dCas9A: 5.83 ± 0.17, n=6; *Scn1a*-dCas9A: 4.83 ± 0.31, n=6; p = 0.02, Chi square test) (**Figure 7G**). The average seizure duration defined by EEG recordings was also shorter (Ctrl-dCas9A: 33.5 ± 2.7 s, n=5; *Scn1a*-dCas9A: 23.9 ± 2.6 s, n=6; p = 0.029, Student's *t*-test) (**Figure 7H**). Finally, we observed a non-significant trend for the spike frequency to be lower in *Scn1a*-dCas9A-treated mice compared to Ctrl-dCas9A treated mice (**Figure 7I, J**).

The upregulation of Nav1.1 during development *in vivo* may be protective against epileptic insults as loss of Nav1.1, in the inverse scenario, is epileptogenic. To test this hypothesis, we performed intraventricular injections of P0 pups with either Ctrl-dCas9A or Scn1A-dCas9A viruses using a pan-neuronal promoter. At P14-17, pups were injected with lipopolysaccharide (LPS) to elicit fever by infection [46,47] followed by repeated low-dose Kainic Acid (KA) injections every 30 minutes, 2 hours later. Epileptic seizures were scored according to the Racine scale and pups were observed every 10 minutes until they reached grade 5, marked by tonic-clonic convulsive seizures (**Figure S8A)**. The time taken to reach grade 5 was used to define the susceptibility to epileptic insults. Pups injected with Scn1a-dCas9A had a higher seizure threshold compared to sham and Ctrl-dCas9A injected animals, confirming the hypothesis that upregulation of Nav1.1 during development is protective against seizures (**Figure S8B**).

In conclusion, these results show that the *Scn1a*-dCas9A system can be efficiently delivered *in vivo* by an AAV-mediated gene transfer in *Scn1a*$^{+/-}$ mice to ameliorate temperature-induced seizures characteristic of this DS mouse strain.

Discussion

DS poses severe challenges for developing an effective therapeutic strategy to control epileptic seizures and associated neurodevelopmental dysfunctions. Currently available antiepileptic drugs are inadequate to suppress recurrent seizures. Furthermore, novel gene therapy approaches for *Scn1a* gene replacement are hampered by the relatively large size of the *Scn1a* gene, which exceeds the packaging cargo of AAV particles. Finally, *Scn1a* transcriptional levels need to be carefully gauged to maintain $Na_v1.1$ protein level compatible with physiological membrane excitability in mature neurons. In light of these significant hurdles, we propose that the dCas9-guided approach for *Scn1a*

gene regulation has invaluable advantages for developing an effective and safe gene therapy strategy for this disease. We identified the sg1P guide, targeting a sequence close to the *Scn1a* proximal promoter, capable of significantly stimulating *Scn1a* expression. A preliminary genomic analysis confirmed that this promoter region is transcriptionally active in the adult mouse and human neurons showing the exact transcriptional start site by CAGE-seq and the crucial epigenetic modifications associated with its functional state. Rapid advances in knowledge of the transcriptional and epigenetic state of the regulatory elements across the genome of neurons will improve the design of effective guides. Importantly, our data provide evidence that this dCas9-based activation system can further stimulate Scn1a increasing its basal expression in young post-mitotic neurons. Surprisingly, we could not detect a significant increase in Scn1a expression in mature wild type neurons while it was evident in Scn1a+/- neurons at both mRNA and protein level upon Scn1a-dCas9A treatment. Considering that approximately 70% of the newly synthesized Nav1.1 constitute a metabolically stable intracellular pool of protein and only 30% is trafficked to the plasma membrane and AIS[48] we can speculate that excessive accumulation of Nav1.1 induces a negative regulation on Scn1a transcript that cannot be overcome even by Scn1a-dCas9A treatment in a wild-type situation. Conversely in *Scn1a*$^{+/-}$ condition, only half of the protein is produced, and this "saturation" is not achieved. In light of this, we propose that the total amount of Nav1.1 channel available in the cell can exert a control by repressing transcription or destabilizing Scn1a mRNA. Further studies are required to determine the details of this regulation and to assess whether stimulation of *Scn1a* gene expression alters the chromatin marks within the promoter region with specific histone modifications associated with this particular transcriptional state. These results have valuable implications for the manipulation of gene expression in the adult brain, providing a tool for a targeted and tunable transcriptional regulation of potentially any genetic element. We achieved good gene transcriptional activation using the dCas9 fused with the effector domains VP64 or VP160. However, recent studies have identified novel transactivators that can elicit higher levels of gene activation[29,34,49]. The establishment of different Cas9 activator systems, each of them with its own advantages, can provide an invaluable toolbox for obtaining the right fine tuning of the transcriptional levels adequate for each specific application. Using global RNA sequencing, we showed that targeted *Scn1a* gene activation was exquisitely specific with no detectable off-target gene activation in primary neurons. These data reveal the high specificity of this approach that will contribute to the high safety level for its future therapeutic applications. In fact, both the new models for accurate prediction of sgRNA off-targets, and the strict requirement for targeting promoter regions close to the transcriptional starting site, contribute to elevate the level of specificity of this approach. Additionally, the use of the dCas9 eliminates the risks of DNA cleavage and its

consequences in post-mitotic neurons that have lost the ability to activate homology-directed repair mechanisms to resolve DNA damage[50,51]. Importantly, dCas9-based stimulation of *Scn1a* expression led to a significant increase of membrane-associated $Na_v1.1$ protein levels that restored correct functioning of DS mutant inhibitory interneurons *in vitro*. Our approach did not distinguish between the two *Scn1a* alleles and also stimulated the expression of the mutant *Scn1a* allele (R1407X). Multiple studies have confirmed that the great majority of the *SCN1A* mutations are loss-of-function and thereby have a negligible effect since they will not produce any stable protein capable of functioning at the neuronal membrane[10]. However, few mutations in SCN1A have been hypothesized from *in vitro* studies to cause the disease through a gain-of-function mechanism[52]. We anticipate that in these particular cases our approach would not be of any advantage. Neuropathological studies have showed that even in advanced stages of the disease there is no evident sign of neuronal cell loss in the patients[53]. These observations strongly imply that dysfunctional interneurons can potentially recover their activity whenever sufficient amount of $Na_v1.1$ channel is available and indicate that at least some DS pathological defects are reversible. Altogether, these results raise the prospective of a cure for this disease even when pathological manifestations are already evident.

In this study, the different elements of the dCas9 activation system were packaged in two different AAVs, but designed to provide an interdependent expression of the different genetic elements. Considering that DS globally affects forebrain interneurons, we carried out AAV intracerebroventricular injections in neonatal mouse pups to cover the entire forebrain structures with a single treatment. In patients, as symptom onset generally occurs within the first two years of life and some more time is required to ascertain *Scn1a* gene mutation by exon sequencing, a later delivery of gene therapy will be required. Nevertheless, the recent discovery of new AAV synthetic serotypes capable of crossing the blood-brain barrier from the bloodstream might open new opportunities for the delivery of therapeutic AAVs for treating CNS disorders. In this respect, peripheral injections of AAV9 in infants with Spinal Muscular Atrophy (SMA), a devastating infantile neurological disorder affecting spinal motor neurons, have recently achieved substantial and long-term clinical benefits[54]. In fact, a single intravenous infusion of the AAV9 expressing the corrected gene resulted in wide protection of the motor skills for extensive period of time and longer survival[54]. This unprecedented clinical success for SMA with a systemic AAV gene therapy approach might facilitate the introduction of a similar strategy to treat other incurable neurological infantile disorders and DS in particular.

Our gene therapy strategy was targeted selectively to forebrain interneurons using the small Dlx5/6 enhancer that has been shown to reliably deliver reporter genes within these neuronal classes[44,45].

Similarly, we reported that this regulatory element ensured restricted expression of the transgenes in the GAD67-GFP neuronal sub-population also in DS adult mice. Even though *Scn1a* is also expressed in subpopulations of cortical excitatory neurons, our strategy almost completely avoided *Scn1a* gene activation in these cells. Nevertheless, *Scn1a* deletion in this neuronal population does not induce noticeable abnormalities in mice, while it ameliorates the pathological phenotype of mice with *Scn1a* deletion in GABAergic neurons[13]. *Scn1a* expression levels are likely different in cortical excitatory and inhibitory neurons and our approach does not allow to deliver different levels of gene activation in different neuronal subtypes. Thus, we considered it safer to employ the Dlx5/6 enhancer to target exclusively the neuronal population whose dysfunctions are leading to the pathological manifestations. The possibility that transduction of extra-cortical interneurons may impact on the treatment efficacy need to be considered. Alternatively, a more selective promoter driving the expression of *Scn1a*-dCas9A system only in cortical interneurons and not in other interneurons (i.e striatal) could be exploited. The *Scn1a* gene activation system attenuated induced epileptic seizures in terms of threshold temperature, total duration, overall clinical severity and recovery period. However, seizures were not completely suppressed. The results can be explained by the relatively low co-infection efficiency of the two separate AAVs in the interneuron population reaching around 20% in the injected area. In fact, the considerable size of the SpCas9 requires the use of two independent AAVs to assemble all the elements for the activation system. Thus, future work is necessary to improve this strategy to package all the system in a unique AAV vector by using significantly smaller Cas9 orthologs such as the SaCas9[55], GeoCas9[56] or CjCas9[57]. Once the AAV vector for Scn1a-dCas9A treatment will be optimized, it would be interesting to test its effect also on the survival rate and spontaneous seizure number and severity in Dravet miceIn conclusion, we showed that the dCas9 activation system can be tailored to obtain a robust and highly specific activation of the *Scn1a* gene both in cultured neurons and in the brain tissue. Moreover, the dCas9 activation system can be packaged into AAVs to establish a gene therapy approach for treating DS mice and obtaining a protection from temperature-induced epileptic seizures. A similar approach can be then considered for other haploinsufficient genetic disorders where stimulation of the wild-type allele can rescue the molecular dysfunctions and lead to a clinical benefit.

Experimental Procedures

Bioinformatics analysis

Transcriptomics and Epigenetics NGS data were downloaded from the Encyclopedia of DNA Elements (ENCODE)[58] and the Functional ANnoTation Of the Mammalian genome (FANTOM)[59] databases. Tracks are visualized along the mm10 mouse reference genome with the Integrative Genome Viewer (IGV)[60].

Molecular cloning

sgRNAs were cloned in a LV-U6 vector as previously described. Ef1alpha-dCas9VP160-T2A-PuroR, was generated from pAC94-pmax-dCas9VP160-2A-puro a gift from Jaenisch R. (Addgene plasmid # 48226)[61]. dCas9VP160-2A-puro cassette was cut with AgeI and inserted in TetO-FUW vector digested with AgeI. The dCas9VP160-2A-puro cassette was restriction digested with with HpaI/AfeI and blunt cloned into Ef1alpha- GFP promoter where GFP was removed by SmaI/EcoRV digestion. Ef1alpha-dCas9VP160-T2A-GFP was obtained by restriction digestion of Ef1alpha-dCas9VP160-T2A-PuroR with AscI/XbaI; the VP160-T2A fragment was obtained by AscI/XhoI digestion from Ef1alpha-dCas9VP160-T2A-Puro^R while GFP fragment was PCR amplified with primers containing XhoI/XbaI restritction sites; the vector and the two fragments were ligated together.

LV-TRE-dCas9VP160-T2A-tdTomato was obtained from TetO-FUW dCas9VP160-2A-puro digested with AscI/XbaI; the VP160-T2A fragment was obtained by AscI/XhoI digestion from Ef1alpha-dCas9VP160-T2A-Puro^R while tdTomato fragment was PCR amplified with primers containing XhoI/XbaI restritction sites; the vector and the two fragments were ligated together. LV-sgRNA-hPGK-rtTA vector was obtained digesting LV-U6-sgRNA with BamHI and cloning rtTA fragment BamHI digested from LV-hPGK-rtTA. The intermediate LV-U6-rtTA was ClaI-XhoI digested and the PGK promoter was PCR amplified with primers with ClaI/XhoI and then cloned. AAV-TRE-dCas9-VP64 was obtained by restriction digestion of AAV-SpCas9 (Kind gift of Zhang F., Addgene # PX551)[51] where Mecp2 promoter was removed by XbaI/AgeI digestion and TRE promoter was amplified with following primers: FWXbaI: GCTCTAGACCAGTTTGGTTAGATCTC and RV AgeI GCACCGGTGCGATCTGACGGTTCACT. SpCas9 was removed with AgeI/EcoRI and Cas9m4-VP64 (kind gift of Church G., addgene # 47319)[26] was digested with AgeI EcoRI. The VP64 fragment was PCR amplified with following primers with ecoRI sites:

F: GATCATCGAGCAAATAAGCGAATTCTC and

R: gctaaGAATTCTTA-TCTAGAGTTAATCAGCATG.

Virus production

Lentiviruses were produced as previously described[62]. For AAV production, replication-incompetent, recombinant viral particles were produced in 293T cells by polyethylenimine (PEI) (Polyscience) co-transfection of three different plasmids: transgene-containing plasmid, packaging plasmid for rep and cap genes, and pAdDeltaF6 for the three adenoviral helper genes. The cells and supernatant were harvested at 120 hr. Cells were lysed in Tris buffer (50 mM Tris, pH 8.5, and 150 mM NaCl; Sigma-Aldrich) by repetitive freeze-thawing cycles (3 times), lysed in Tris buffer, and combined with correspondent cell lysates. To clarify the lysate, benzonase treatment was performed (250 U/mL, 37°C for 30 min; Sigma-Aldrich) in the presence of 1 mM $MglCl_2$ (Sigma- Aldrich) and cellular debris separated by centrifugation (2,000 × *g*, 30 min). The viral phase was isolated by an iodixanol step gradient (15%, 25%, 40%, 60% Optiprep; Sigma-Aldrich) in the 40% fraction and concentrated in PBS with a 100,000 molecular weight cut-off concentrator (Vivaspin 20; Sartorius Stedim). Virus titers were determined by measuring the number of DNase I-resistant viral particles, using qPCR with linearized genome plasmid as a standard. The TRE-dCas9-VP64 has been produced by VectorBuilder Ltd (Ca, United States).

Mice

Mice were maintained at the San Raffaele Scientific Institute Institutional mouse facility (Milan, Italy). *Scn1a*$^{+/-}$[10] were backcrossed with 129Sv mice, while GAD67-GFP[63] , *Pvalb*$^{tm1(cre)Arbr}$ (JAX 017320, PV-Cre) and Rosa26$^{LSL\text{-}tdTomato}$ (JAX 007909, Ai9) mice were backcrossed with C57BL/6N. PV-Cre$^{+/+}$ were crossed to Ai9$^{+/+}$ to generate PV-Cre$^{+/+}$ Ai9$^{+/+}$. Those mice were then crossed with 129Sv.Scn1a$^{+/-}$ mice to generate Scn1a $^{+/-}$; PV-Cre$^{+/-}$ Ai9$^{+/-}$ mice and Scn1a$^{+/-}$;PV-Cre$^{+/-}$ Ai9$^{+/-}$. All procedures were performed according to protocols approved by the internal institutional animal care and use committee (IACUC) and reported to the Italian Ministry of Health according to the European Commission Council Directive 2010/63/EU and in accordance with the UK Animals (Scientific Procedures) Act of 1986.

Cell cultures and primary neuron derivation

P19 cells were cultured in alpha-MEM (Sigma-Aldrich), supplemented with 10% fetal bovine serum (Sigma- Aldrich), 1% non-essential amino acids (Gibco), 1% sodium pyruvate (Sigma-Aldrich), 1% glutamine (Sigma-Aldrich), and 1% penicillin/streptomycin (Sigma-Aldrich). Cells were split every 2-3 days using 0.25% trypsin (Sigma-Aldrich). For transfection, Lipofectamine 300 (Thermo Fisher

Scientific) was used according to the manufacturer's protocol. Primary cultures of mouse embryonic hippocampal neurons were prepared from E17.5 embryos or P0 pups derived from GAD67-GFP knock-in and *Scn1a*$^{+/-}$;GAD67-GFP pregnant females. In the latter case, each brain was processed separately and a skin biopsy was used for genotyping. Briefly, after dissection, hippocampi were enzymatically digested with 0.025% trypsin (Gibco) in Hank's balanced salt solution (HBSS) (Euroclone) for 20 min at 37 °C. Successively, HBSS with trypsin was removed and the hippocampi were washed with plating medium (Neurobasal medium (Gibco) supplemented with 2% B27, 3.3mM glucose, 1% glutamine and penicillin/streptomycin) and mechanically dissociated with a P1000-pipette to obtain a homogeneous cell suspension. Cells were then plated on poly-L- lysine (PLL) (0.1 mg/ml) coated plates and coverslips. LV infection was performed at DIV 1 and neurons were used at DIV 10 or 21 for electrophysiology, Western blot analysis and immunofluorescence. For recordings from interneurons, cells patched showed co-localization of both green (indicating interneurons) and red (indicating successful lentiviral transduction) fluorescent signal.

Western blotting

Total cerebral cortex from *Scn1a*$^{+/-}$ mice, wild-type mice, and primary neurons were homogenized using the Mem-PER™ Plus Membrane Protein Extraction Kit (Thermo Fisher) according to manufacturer's instructions to enrich for the membrane-bound proteins. Western blot analysis was performed on Nupage 4-12% gradient gels (Thermo Fisher) using primary antibodies against the following proteins: anti-$Na_v1.1$ (1:200, Millipore) anti-Calnexin (1:5000, Sigma).

RNA isolation quantitative reverse-transcription PCR

RNA was extracted using TRI Reagent (Merck) according to the manufacturer's instructions. For quantitative RT-PCR (RT-qPCR), cDNA synthesis was obtained using the ImProm-II Reverse Transcription System (Promega), whereafter RT-qPCR was performed in triplicate with custom designed oligos (Supplementary Table 2) using the Titan HotTaq EvaGreen qPCR Mix (no ROX) (BIOATLAS). Analysis of relative expression was performed using the ΔΔCt method.

RNA-sequencing

RNA libraries were generated starting from 1 microgram of total RNA extracted from Ctrl- dCas9A and *Scn1a*-dCas9A neurons. RNA quality was assessed by using a Tape Station instrument (Agilent). To avoid over-representation of 3'ends, only high-quality RNA with a RNA Integrity Number (RIN) ≥ 8 was used. RNA was processed according to the QuantSeq 3' mRNA-Seq Library Prep Kit protocol. The libraries were sequenced on an Illumina HiSeq 2500 with 50bp stranded

reads using Illumina TruSeq technology. Image processing and basecall were performed using the Illumina Real Time Analysis Software. Fastq files were aligned to the mouse genome (NCBI37/mm9) with Bowtie2[64]. Differential gene expression and functional enrichment analyses were performed with DESeq2[65], respectively. Statistical analysis was performed with the SPSS statistical package (IBM). Data were deposited in the NCBI Gene Expression Omnibus repository with the NCBI GEO: GSE111436 ~~GEO ID~~.

Deep sequencing data analysis

Indexed paired-end libraries were generated starting from 1 microgram of PCR amplicon spanning $Scn1a^{RX}$ gene mutation[10] performed on cDNA obtained from retrotranscribed (RT) RNA using Illumina TruSeq Nano DNA Library Prep kits, according to manufacturer instructions. Libraries were sequenced on an Illumina MiSeq. FASTQ reads were aligned to the hg38 human reference genome with Bowtie2. Alignments were visualized and quantified with the IGV genome browser.

In vitro electrophysiology

Current steps. For current-clamp recordings, the internal solution contained (in mM): 126 K-gluconate, 4 NaCl, 1 $MgSO_4$, 0.02 $CaCl_2$, 0.1 BAPTA, 15 Glucose, 5 HEPES, 3 ATP-Na_2, 0.1 GTP-Na, pH 7.3. The extracellular (bath) solution contained (in mM): 2 $CaCl_2$, 140 NaCl, 1 $MgCl_2$, 10 HEPES, 4 KCl, 10 glucose, pH 7.3. D-(−)-2-amino-5-phosphonopentanoic acid (D- AP5; 50 μM), 6-cyano-7-nitroquinoxaline-2,3-dione (CNQX; 10 μM) and picrotoxin (PTX; 30 μM) were added to block synaptic transmission. Experiments were performed at room temperature (22-24 °C). Transduced cortical and hippocampal interneurons were identified because expressing GAD67-GFP and tdTomato (dCas9A system). Neurons with unstable resting potential (or > -50mV), bridge-balance > 15 MΩ and/or holding current >200 pA at -70mV were discarded. Bridge balance compensation was applied and the resting membrane potential was held at -70 mV. Current steps protocols were used to evoke action potentials (APs) injecting 250 ms long depolarizing current steps of increasing amplitude (Δ 10pA, max 280pA). Recordings were acquired using a Multiclamp 700A amplifier (Axon Instruments, Molecular Devices) and a Power3 1401 (CED) interface combined with Signal software (CED), filtered at 10 kHz and digitized at 50 kHz. Passive properties were calculated from the hyperpolarizing steps of the current clamp steps protocol. Input resistance is an average of three steps (2 negative and one positive) and is defined as the as the ΔV/I. Capacitance was calculated in the current clamp hyperpolarizing step as follow: firstly, the resistance was determined as DV/DI (voltage/current), then the cell time constant (tau) was obtained

fitting the voltage changing between baseline and hyperpolarizing plateau. Capacitance was calculated as tau/resistance. Capacitance is time constant of the voltage between the baseline and the plateau during a hyperpolarizing step. Single AP parameters were calculated as previously described[62]. An event was detected as AP if cross 0 mV and if rising slope was >20mV/ms in a range of injected current from 0 pA to 500 pA. All recordings and analysis were carried blinded to vector transduced.

Activity clamp

For activity clamp experiments, current traces in voltage-clamp configuration in presence of 4AP were recorded holding GFP positive interneurons (18 DIV) at -70mV in presence of $GABA_A$ and NMDA blockers. The resulting AMPA-current traces were converted in conductance (G=I/V). Using Signal dynamic clamp software in conjunction with CED Power 1401- 3 (CED) the conductance traces were used to inject currents in interneurons in current clamp configuration. During recordings, the voltage of the patched neurons was read in real time, and used to calculate the current to be injected from the 4AP conductance trace. In order to compare different cells the conductance threshold was calculated in each neuron prior to each dynamic clamp experiment. For voltage-clamp spontaneous excitatory synaptic activity of the epileptic traces (4AP, 100 µM) and current-clamp recordings in dynamic clamp configuration the internal and the extracellular solutions were the same described above for neuronal whole cell patch clamp recordings. For voltage-clamp recordings in the extracellular solution D-AP5 (50 µM) and PTX (30 µM) were added to block $GABA_A$ and NMDA receptors respectively. For current-clamp recordings D-AP5 (50 µM), CNQX (10 µM) and PTX (30 µM) were added to block NMDA receptors, AMPA receptors and GABAA receptors, respectively. Experiments were performed at room temperature (22-24 °C). For voltage-clamp recordings neurons with unstable resting potential and/or a leak current >100 pA were discarded and neurons were clamped at -70 mV. For current- clamp recordings neurons with unstable resting potential and/or bridge-balance >15 MΩ were discarded. Bridge balance compensation was applied and the resting membrane potential was held at -70 mV. An AMPA conductance step protocol (Erev = 0 mV; τ=1ms; ΔG = 1 nS) was used to find the conductance threshold that elicited an AP and then the epileptic conductance trace was scaled to the 15% of the conductance threshold. Neurons that were unable to generate at least one AP were therefore excluded. The sampling frequencies in voltage and in current clamp configurations were set at 20 kHz to perfectly overlap the conductance traces with the software voltage reading. To analyze the dynamic clamp traces an automatic Matlab script was used[41] to detect events and calculate APs

parameters. An event was selected as AP if its peak crossed 0mV and if its dv/dt was >20. Voltage threshold was calculated as the first point with a derivative >20 V/sec. All recordings and analysis were carried blinded to the transduced vector. Recordings were acquired using a Multiclamp 700A amplifier (Axon Instruments, Molecular Devices, Sunnyvale, CA, USA) and Signal dynamic clamp software in conjunction with CED Power 1401-3 (CED, Cambridge Electronic Design Limited), filtered at 10 kHz and digitized at 50 kHz.

Ex-vivo electrophysiology

Mice were sacrificed after deep isoflurane anesthesia, and brains extracted. 350μm thick coronal sections were cut using a Leica VTS 1000 vibratome. After the cut the slices were allowed to recover for 30 minute at 32°C in modified ACSF containing: 92 mM Sucrose, 87mM NaCl, 2.5 mM KCl, 1.25 mM NaH_2PO_4, 25 mM $NaHCO_3$, 25 mM glucose, mM $CaCl_2$·and 10 mM $MgSO_4$ aerated with 95% O_2 and 5% CO_2 (pH 7.4); slices were then allowed to recover at room temperature for at least 45 minute before recording.

Current-clamp recordings were performed using a MultiClamp 700B amplifier (Molecular Devices) with pCLAMP 10 software. Pipette capacitance and resistance were always compensated. Signals were low-pass filtered at 10 kHz, sampled at 50 –100 kHz; signal was digitized using a Digidata 1550 D/A converter (Molecular Devices).

Cells were held at 30-32°C. The extracellular solution contained (mM): 125 NaCl, 25 $NaHCO_3$, 2 $CaCl_2$, 2.5 KCl, 1.25 NaH_2PO_4, 1 $MgSO_4$, 10 D-glucose, aerated with 95% O_2 and 5% CO_2 (pH 7.4). Patch pipette contained (mM): 124 KH2PO4, 5 KCl, 2$MgCl_2$, 10 NaCl, 10 HEPES, 0.5 EGTA, 2 Na-ATP, 0.2 Na-GTP, pH 7.25 (adjusted with KOH).

Ctrl-and Scn1a-dCas9A PV^+ interneurons were identified via tdTomato and GFP expression, visualized with epifluorescence microscopy. Input/output relationship was determined plotting AP frequency in response to progressive 500 ms 50 pA current step injection. An AP was defined as spikes having rising slope> 20V/s and an amplitude exceeding -15 mV. Maximal steady-state firing frequency was defined as the maximal mean firing frequency in response to a current injection. Input resistance (Rm) was calculated from a -50 pA steps from resting membrane potential. AP amplitude was calculated from AP threshold, defined as the voltage at which the first derivative (dV/dt) of the AP waveform reached 10 mV/ms, to the absolute value of the AP peak for the first spike obtained at the rheobase (defined as the minimal current injection able to elicit neuronal firing, determined through 10pA current steps). Spike width was determined at half-amplitude (Halfwidth) between AP threshold and peak. Spike frequency adaptation (SFA) is calculated as the ratio of the first to the tenth (ISI1/ISI10) inter-spike interval. Maximal rise and

decay slope were defined respective as the maximal and minimal value of the first derivative of the AP waveform.

Intracerebroventricular injections

Neonatal mice were anesthetized in ice for 3 minutes. Five µl of viral suspension containing two AAVs (titer 10^{13} vg/ml) (TRE-dCas9-VP64 and pU6-sgCrtl/sg1P-mDlx5enh-rtTa-T2A-Tomato/GFP, 1:1,) and 0.05% Fast Green FCF (Sigma Aldrich) was injected into lateral ventricles using a Hamilton syringe with a 33-gauge needle. After injections, pups were placed on a warming pad until they regained normal color and movements. Subsequently, they were rubbed with bedding to prevent rejection before reintroducing the mother into the cage. Doxycycline (dox) was administered immediately in drinking water or food. One week after injections mice were genotyped.

Immunostainings

Cells and neurons were fixed ice-cold 4% paraformaldehyde (PFA) in PB for 20 minutes. Mice were anesthetized with ketamine/xylazine and t perfused with 0.1M phosphate buffer (PB) at room temperature (RT) at pH 7.4 with freshly prepared, PFA in PB. Tissues were post-fixed in 4% PFA overnight and then soaked in cryoprotective solution (30% sucrose in PBS). Tissues were sectioned using cryostat after optimal cutting temperature (OCT) compound embedding in dry ice. For immunofluorescence, free- floating 30 µm-thick coronal sections or plated cells were rinsed in PBS and were incubated for 20 min with 2% Triton X-100 and 3% BSA for 1 hr was used to saturate the unspecific binding site before the overnight incubation with the primary antibody (diluted in a solution containing 1% BSA and Triton X-100 at RT). Following incubation, sections were rinsed three times in PBS and incubated for 1 hr with the secondary antibody.

Primary antibodies for the following epitopes were used: RFP (rabbit, 1:500, MBL International), GFP (cicken, 1:500; Molecular Probes), Calbindin (mouse, 1:200; Swant), PV (mouse, 1:500; Swant), SST (rat, 1:200, Millipore), NPY (rabbit, 1:500, Immunostar), VIP (rabbit, 1:500, Immunostar), Map2 (mouse, 1:250 Immunological Science), GABA (rabbit, 1:1000 Sigma-Aldrich), Tra1-60 (mouse, 1:200 Millipore), Oct4 (rabbit, 1:300 Abcam), Sox2 (rabbit, 1:200 Abcam), SMA (mouse, 1:500 Sigma-Aldrich), TUBB3 (mouse, 1:500 Covance), Foxa2 (rabbit, 1:200 Millipore). Slices and cell coverslips were mounted with fluorescent mounting medium (Dako). Images were captured with a Nikon Eclipse 600 fluorescent microscope.

Surgery for electrode implant, seizure induction and EEG

At least five days before recordings, epidural stainless-steel screw electrodes (0.9 mm diam./3 mm long) were surgically implanted under intraperitoneal anaesthesia (100 mg/kg ketamine, 10 mg/kg xylazine) and secured using dental cement (Ketac Cem, ESPE Dental AG, Seefeld, Germany). Two active electrodes were placed on right and left parietal areas (2mm lateral to midline, 1mm posterior to bregma) and one over the occipital area (1mm posterior to lambda) as a common reference.

For video-EEG recording, the implanted electrodes were connected via flexible cables to an amplifier and EEG signal was sampled at 256 Hz, coded with 16 bits and digitally saved using System Plus device (Micromed, Mogliano Veneto, Italy). In order to obtain a good signal-to-noise ratio for seizure displaying, after the acquisition EEG traces were bandpass filtered between 0.3 and 10 Hz. Video-EEG recordings were inspected to detect seizures, defined as high- amplitude (at least twice the baseline) rhythmic discharges lasting at least 5 seconds. We defined the beginning of the seizure as the first EEG change; the end of the seizure was defined as the end of ictal EEG activity. To induce seizures, we adopted a protocol modified from Oakley and colleagues[16]. Mice were placed in a glass beaker and heated with an infrared heat lamp HL-1 (Phisitemp, Clifton, New Jersey) controlled by a TCAT-2DF thermocontroller (Phisitemp, Clifton, New Jersey). Mice rectal temperature was continuously monitored with a RET-4 probe (Phisitemp, Clifton, New Jersey). Seizures were identified by EEG recording and video analysis. Firstly, mice were recorded at baseline for 15 minutes, then seizures were evoked by progressively increasing mice body temperature by 0.5 °C every 30 s. The heating bulb was then promptly switched off to allow mice recovery; mice were then monitored until EEG and temperature returned to the baseline or until death occurred.

For EEG analysis, Neuroscore (Data Sciences International, S. Paul, Minnesota) was used. For spike detection, EEG traces were first bandpass filtered between 5 and 70 Hz. Threshold temperature, seizure duration, number of spikes during the attack and spike frequency were considered. Spikes were detected by threshold analysis then visually inspected to reject artifacts. All recordings and analysis were carried blinded to the transduced viruses. Seizure severity was scored using a modification of the Racine scale[66].

KA-induced febrile seizures in pups

A rectal temperature probe was used in P14-17 pups to measure the basal body temperature before each injection. A single LPS injection (2µg/mouse, Sigma L4516) was administrated via IP 2 hours before the experiment to induce fever and increase the temperature of the pups. Low-dose IP KA injections (5mg/Kg, Tocris 0222) were performed every hour and seizures scored using the Racine scale every 10 minutes. Mice were culled after grade 5 was reached and the time taken to reach

grade 5 was used as a read-out of seizure susceptibility. Seizure scoring was performed blinded to the identity of the virus injected.

Statistical analysis

The results were analyzed with GraphPad Prism. Mean comparisons among different groups were performed with the Student's *t*-test or two-way ANOVA followed by the Bonferroni's multiple comparison test. In case of non-normally distributed data, median comparisons between two groups were performed with the Mann Whitney *U*-test. The normality in the data distribution was assessed using the D'Agostino and Pearson omnibus test. For seizure score comparison, the Chi-square test was employed. Individual statistical analyses and details of experimental design are described in detail alongside each experiment in the Results section and Figure legends.

References

1. Kullmann, D. M. Neurological Channelopathies. *Annu. Rev. Neurosci.* **33**, 151–172 (2010).
2. DRAVET, C. Dravet syndrome history. *Dev. Med. Child Neurol.* **53**, 1–6 (2011).
3. Meisler, M. H. & Kearney, J. a. Date - 4th Nov . 08 Review series Presenter - Anand Sodium channel mutations in epilepsy and other neurological disorders Date - 4th Nov . 08 Presenter - Anand. *J. Clin. Invest.* **115**, (2005).
4. Nickels, K. C. & Wirrell, E. C. Cognitive and Social Outcomes of Epileptic Encephalopathies. *Semin. Pediatr. Neurol.* **24**, 264–275 (2017).
5. Kasperaviciute, D. *et al.* Epilepsy, hippocampal sclerosis and febrile seizures linked by common genetic variation around SCN1A. *Brain* **136**, 3140–50 (2013).
6. Cetica, V. *et al.* Clinical and genetic factors predicting Dravet syndrome in infants with SCN1A mutations. *Neurology* **88**, 1037–1044 (2017).
7. Marini, C. *et al.* The genetics of Dravet syndrome. *Epilepsia* **52**, 24–29 (2011).
8. Yu, F. H. *et al.* Reduced sodium current in GABAergic interneurons in a mouse model of severe myoclonic epilepsy in infancy. *Nat. Neurosci.* **9**, 1142–1149 (2006).
9. Han, S. *et al.* Autistic-like behaviour in Scn1a +/− mice and rescue by enhanced GABA-mediated neurotransmission. *Nature* **489**, 385–390 (2012).
10. Ogiwara, I. *et al.* Nav1.1 Localizes to Axons of Parvalbumin-Positive Inhibitory Interneurons: A Circuit Basis for Epileptic Seizures in Mice Carrying an Scn1a Gene Mutation. *J. Neurosci.* **27**, 5903–5914 (2007).

11. Ito, S. *et al.* Mouse with Nav1.1 haploinsufficiency, a model for Dravet syndrome, exhibits lowered sociability and learning impairment. *Neurobiol. Dis.* **49**, 29–40 (2013).

12. Hedrich, U. B. S. *et al.* Impaired action potential initiation in GABAergic interneurons causes hyperexcitable networks in an epileptic mouse model carrying a human Na(V)1.1 mutation. *J. Neurosci.* **34**, 14874–89 (2014).

13. Ogiwara, I. *et al.* Nav1.1 haploinsufficiency in excitatory neurons ameliorates seizure-associated sudden death in a mouse model of Dravet syndrome. *Hum. Mol. Genet.* **22**, 4784–4804 (2013).

14. Tai, C., Abe, Y., Westenbroek, R. E., Scheuer, T. & Catterall, W. A. Impaired excitability of somatostatin- and parvalbumin-expressing cortical interneurons in a mouse model of Dravet syndrome. *Proc. Natl. Acad. Sci.* **111**, E3139–E3148 (2014).

15. Tatsukawa, T., Ogiwara, I., Mazaki, E., Shimohata, A. & Yamakawa, K. Impairments in social novelty recognition and spatial memory in mice with conditional deletion of Scn1a in parvalbumin-expressing cells. *Neurobiol. Dis.* **112**, 24–34 (2018).

16. Oakley, J. C., Kalume, F., Yu, F. H., Scheuer, T. & Catterall, W. A. Temperature- and age-dependent seizures in a mouse model of severe myoclonic epilepsy in infancy. *Proc. Natl. Acad. Sci.* **106**, 3994–3999 (2009).

17. Wirrell, E. C. Treatment of Dravet Syndrome. *Can. J. Neurol. Sci. / J. Can. des Sci. Neurol.* **43**, S13–S18 (2016).

18. Chiron, C. & Dulac, O. The pharmacologic treatment of Dravet syndrome. *Epilepsia* **52**, 72–75 (2011).

19. Griffin, A. *et al.* Clemizole and modulators of serotonin signalling suppress seizures in Dravet syndrome. *Brain* aww342 (2017). doi:10.1093/brain/aww342

20. Sourbron, J. *et al.* Serotonergic Modulation as Effective Treatment for Dravet Syndrome in a Zebrafish Mutant Model. *ACS Chem. Neurosci.* **7**, 588–98 (2016).

21. Devinsky, O., Cross, J. H. & Wright, S. Trial of Cannabidiol for Drug-Resistant Seizures in the Dravet Syndrome. *N. Engl. J. Med.* **377**, 699–700 (2017).

22. Murlidharan, G., Samulski, R. J. & Asokan, A. Biology of adeno-associated viral vectors in the central nervous system. *Front. Mol. Neurosci.* **7**, (2014).

23. Kay, M. A., Glorioso, J. C. & Naldini, L. Viral vectors for gene therapy: the art of turning infectious agents into vehicles of therapeutics. *Nat. Med.* **7**, 33–40 (2001).

24. Wright, A. V, Nuñez, J. K. & Doudna, J. A. Biology and Applications of CRISPR Systems: Harnessing Nature's Toolbox for Genome Engineering. *Cell* **164**, 29–44 (2016).

25. Hsu, P. D., Lander, E. S. & Zhang, F. Development and Applications of CRISPR-Cas9 for Genome Engineering. *Cell* **157**, 1262–1278 (2014).

26. Mali, P. *et al.* CAS9 transcriptional activators for target specificity screening and paired nickases for cooperative genome engineering. *Nat. Biotechnol.* **31**, 833–838 (2013).

27. Dominguez, A. A., Lim, W. A. & Qi, L. S. Beyond editing: repurposing CRISPR–Cas9 for precision genome regulation and interrogation. *Nat. Rev. Mol. Cell Biol.* **17**, 5–15 (2016).

28. Sander, J. D. & Joung, J. K. CRISPR-Cas systems for editing, regulating and targeting genomes. *Nat. Biotechnol.* **32**, 347–55 (2014).

29. Liu, J. *et al.* ORIGINAL ARTICLE CRISPR / Cas9 facilitates investigation of neural circuit disease using human iPSCs : mechanism of epilepsy caused by an SCN1A loss-of-function mutation. (2016). doi:10.1038/tp.2015.203

30. Liao, H.-K. *et al.* In Vivo Target Gene Activation via CRISPR/Cas9-Mediated Trans-epigenetic Modulation. *Cell* **171**, 1495-1507.e15 (2017).

31. Hilton, I. B. *et al.* Epigenome editing by a CRISPR-Cas9-based acetyltransferase activates genes from promoters and enhancers. *Nat. Biotechnol.* **33**, 510–517 (2015).

32. Liu, X. S. *et al.* Editing DNA Methylation in the Mammalian Genome. *Cell* **167**, 233-247.e17 (2016).

33. Zhou, H. *et al.* In vivo simultaneous transcriptional activation of multiple genes in the brain using CRISPR–dCas9-activator transgenic mice. *Nat. Neurosci.* **21**, 440–446 (2018).

34. Konermann, S. *et al.* Genome-scale transcriptional activation by an engineered CRISPR-Cas9 complex. *Nature* **517**, 583–8 (2015).

35. Simeonov, D. R. *et al.* Discovery of stimulation-responsive immune enhancers with CRISPR activation. *Nature* **549**, 111–115 (2017).

36. Gilbert, L. A. *et al.* CRISPR-Mediated Modular RNA-Guided Regulation of Transcription in Eukaryotes. *Cell* **154**, 442–451 (2013).

37. Kearns, N. A. *et al.* Cas9 effector-mediated regulation of transcription and differentiation in human pluripotent stem cells. *Development* **141**, 219–223 (2014).

38. Matharu, N. *et al.* CRISPR-mediated activation of a promoter or enhancer rescues obesity

caused by haploinsufficiency. *Science (80-.).* **363**, eaau0629 (2019).

39. Nakayama, T. *et al.* Deletions of SCN1A 5′ genomic region with promoter activity in Dravet syndrome. *Hum. Mutat.* **31**, 820–829 (2010).

40. Grubb, M. S. & Burrone, J. Activity-dependent relocation of the axon initial segment fine-tunes neuronal excitability. *Nature* **465**, 1070–1074 (2010).

41. Morris, G. *et al.* Activity Clamp Provides Insights into Paradoxical Effects of the Anti-Seizure Drug Carbamazepine. *J. Neurosci.* **37**, 5484–5495 (2017).

42. Cheah, C. S. *et al.* Correlations in timing of sodium channel expression, epilepsy, and sudden death in Dravet syndrome. *Channels* **7**, (2013).

43. Hammond, S. L., Leek, A. N., Richman, E. H. & Tjalkens, R. B. Cellular selectivity of AAV serotypes for gene delivery in neurons and astrocytes by neonatal intracerebroventricular injection. *PLoS One* **12**, e0188830 (2017).

44. Dimidschstein, J. *et al.* A viral strategy for targeting and manipulating interneurons across vertebrate species. *Nat. Neurosci.* **19**, 1743–1749 (2016).

45. Stühmer, T., Puelles, L., Ekker, M. & Rubenstein, J. L. R. Expression from a Dlx gene enhancer marks adult mouse cortical GABAergic neurons. *Cereb. Cortex* **12**, 75–85 (2002).

46. Eun, B.-L., Abraham, J., Mlsna, L., Kim, M. J. & Koh, S. Lipopolysaccharide potentiates hyperthermia-induced seizures. *Brain Behav.* **5**, n/a-n/a (2015).

47. Heida, J. G., Teskey, G. C. & Pittman, Q. J. Febrile convulsions induced by the combination of lipopolysaccharide and low-dose kainic acid enhance seizure susceptibility, not epileptogenesis, in rats. *Epilepsia* **46**, 1898–905 (2005).

48. Schmidt, J. W. & Catterall, W. A. Biosynthesis and processing of the α subunit of the voltage-sensitive sodium channel in rat brain neurons. *Cell* **46**, 437–445 (1986).

49. Chavez, A. *et al.* Comparison of Cas9 activators in multiple species. *Nat. Methods* **13**, 563–567 (2016).

50. Staahl, B. T. *et al.* Efficient genome editing in the mouse brain by local delivery of engineered Cas9 ribonucleoprotein complexes. *Nat. Biotechnol.* **35**, 431–434 (2017).

51. Swiech, L. *et al.* In vivo interrogation of gene function in the mammalian brain using CRISPR-Cas9. *Nat. Biotechnol.* **33**, 102–106 (2015).

52. Rhodes, T. H., Lossin, C., Vanoye, C. G., Wang, D. W. & George, A. L. Noninactivating

voltage-gated sodium channels in severe myoclonic epilepsy of infancy. *Proc. Natl. Acad. Sci.* **101**, 11147–11152 (2004).

53. Catarino, C. B. *et al.* Dravet syndrome as epileptic encephalopathy: evidence from long-term course and neuropathology. *Brain* **134**, 2982–3010 (2011).

54. Mendell, J. R. *et al.* Single-Dose Gene-Replacement Therapy for Spinal Muscular Atrophy. *N. Engl. J. Med.* **377**, 1713–1722 (2017).

55. Chen, B. *et al.* Expanding the CRISPR imaging toolset with *Staphylococcus aureus* Cas9 for simultaneous imaging of multiple genomic loci. *Nucleic Acids Res.* **44**, e75–e75 (2016).

56. Harrington, L. B. *et al.* A thermostable Cas9 with increased lifetime in human plasma. *Nat. Commun.* **8**, 1424 (2017).

57. Kim, E. *et al.* In vivo genome editing with a small Cas9 orthologue derived from Campylobacter jejuni. *Nat. Commun.* **8**, 14500 (2017).

58. Davis, C. A. *et al.* The Encyclopedia of DNA elements (ENCODE): data portal update. *Nucleic Acids Res.* **46**, D794–D801 (2018).

59. Carninci, P. *et al.* Genome-wide analysis of mammalian promoter architecture and evolution. *Nat. Genet.* **38**, 626–635 (2006).

60. Thorvaldsdóttir, H., Robinson, J. T. & Mesirov, J. P. Integrative Genomics Viewer (IGV): high-performance genomics data visualization and exploration. *Brief. Bioinform.* **14**, 178–92 (2013).

61. Cheng, A. W. *et al.* Multiplexed activation of endogenous genes by CRISPR-on, an RNA-guided transcriptional activator system. *Cell Res.* **23**, 1163–1171 (2013).

62. Colasante, G. *et al.* Rapid Conversion of Fibroblasts into Functional Forebrain GABAergic Interneurons by Direct Genetic Reprogramming. *Cell Stem Cell* **17**, 719–734 (2015).

63. Tamamaki, N. *et al.* Green fluorescent protein expression and colocalization with calretinin, parvalbumin, and somatostatin in the GAD67-GFP knock-in mouse. *J. Comp. Neurol.* **467**, 60–79 (2003).

64. Langmead, B., Trapnell, C., Pop, M. & Salzberg, S. L. Ultrafast and memory-efficient alignment of short DNA sequences to the human genome. *Genome Biol.* **10**, R25 (2009).

65. Love, M. I., Huber, W. & Anders, S. Moderated estimation of fold change and dispersion for RNA-seq data with DESeq2. *Genome Biol.* **15**, 550 (2014).

66. Velíšková, J. & Velíšek, L. Behavioral Characterization and Scoring of Seizures in Rodents. *Model. Seizures Epilepsy* 111–123 (2017). doi:10.1016/B978-0-12-804066-9.00009-2

Acknowledgements

We are thankful to Dr. K. Yamakawa for Scn1a mutant mice, L. Muzio, S. Levi and D. Zacchetti for providing valuable reagents, S. Comai and M. Simonato for sharing of the *in vivo* EEG recording instrumentation, C. Butti and E. Fraviga for technical help, D. Bonanomi, and all members of the Broccoli's lab for helpful discussion. We acknowledge the FRACTAL core facility for expert supervision in flow-cytometry. This work was supported by the "Associazione Gruppo Famiglie Dravet" to V.B., European Union FP7 Integrating Project "Desire" (Grant agreement n. 602531) to F.B. and V.B., CARIPLO Foundation (2016-0532) and the Italian Ministry of Health (GR-2016-02363972) to G.C., the Marie Curie individual fellowship to G.L., the MRC Gene therapy grant to S.S. and D.M.K.

Author contributions

G.C. and G.L performed the experiments and analyzed data; C.D.B. designed and tested the sgRNAs and *Scn1a* transcriptional activation; J.C. performed in vivo WT experiments; N.V., G.M. and S.Bi. executed viral injections in mice; L.M. developed the computational analysis; S.Br., V.C. S.M. and L.L. performed and analyzed the in vivo EEG recordings; S.G. produced AAVs; T.C. contributed to *in vitro* electrophysiology; F.B. contributed in analyzing the electrophysiological recordings; S.S. and D.K. contributed in designing the experiments; V.B. supervised, coordinated and supported the project and wrote the paper with G.C. and G.L.

Competing financial interests

The authors declare no competing interests.

Figure Legends

Figure 1 | sgRNA designing and screening for stimulating *Scn1a* gene expression with the dCas9 activation system in P19 cells.

A, Schematic representation of the *Scn1a* gene with distal **(B)** and proximal **(C)** promoter regions where the positions of the sgRNAs selected for this screening are highlighted. **D,** Experimental setting for the sgRNA screening in P19 cells and schematic representation of the constructs employed for cell lipofection. One day after plating, P19 cells were lipofected, and the subsequent day GFP expression was ascertained. At 3 DIV the cells were processed for RNA extraction. **E,F,** Quantitative RT-PCRs for *Scn1a* mRNA levels performed on RNA extracted from P19 cells lipofected with dCas9VP160-T2A-GFP together with sgRNAs targeting the distal **(E)** or proximal **(F)** promoter. Data are normalized on the 18S rRNA and relative to control sgCtrl lipofected cells. sg1p induces significant up-regulation of *Scn1a* compared to sgCtrl ($n = 6$, $p < 0.0001$, one-way ANOVA followed by Bonferroni multi comparison tests). Data are shown as mean ± s.e.m with dots representing individual samples.

Figure 2 | dCas9-VP160/sg1P potentiates *Scn1a* gene transcription in primary hippocampal neurons.

A, Schematic drawing depicting the experimental setting to deliver the Ctrl- and *Scn1a*-dCas9A system in primary neurons. Hippocampal neurons were derived from E17.5 embryos and the day after plating were co-transduced with two distinct lentiviruses (LV) carrying Ef1a-dCas9-VP160-T2A-GFP and pU6-sg1P or pU6-sgCtrl guides, respectively. **B**, Representative image of anti-GFP immunofluorescence at 10 DIV and quantification of GFP^+ transduced neurons over the total cell number, scale bar 50um. **C**, Representative FACS images of GFP^+ neurons transduced with either the sgCtrl- or sg1P-dCas9 activation system. **D,** RT-qPCR reveal the increased *Scn1a* transcriptional levels in hippocampal neurons infected with the sg1P with respect to sgCtrl conditions ($n = 6$, $p = 0.0002$, Student's *t*-test). Data are shown as mean ± s.e.m. with dots representing individual samples. **E,** Schematic setting of the E17.5 neurons transduced with a single lentivirus (LV) carrying both the pU6-sgRNA cassette and dCas9-VP160-T2A-GFP sequence under the control of the EF1alpha-core promoter. **F**, Anti-GFP immunofluorescence at 10 DIV and relative quantification of transduced GFP^+ cells over total showing that a single LV reaches transduction efficiency of 75%, scale bar 50um . **G** RT-qPCR for *Scn1a* with primers amplifying the first (ExonA) and second 5'-UTR exon (ExonB). Data are normalized on 18S rRNA and expressed as relative to sgCtrl. (ExonA, sg1p vs sgCtrl: $p = 0.7353$; ExonB, sg1p vs sgCtrl: $p < 0.0001$, Student's *t*-test). **H**, left, Western blot for $Na_V1.1$ and Calnexin on protein lysates from Ctrl-dCas9A and *Scn1a*-dCas9A treated neurons at 10 DIV; right, quantification obtained through densitometry and normalized on Calnexin levels and expressed as *Scn1a*- dCas9A relative to Ctrl-dCas9A (data are shown as mean ± s.e.m. with dots representing individual samples); $n = 4$, sg1p vs sgCtrl:$p = 0.03$, Student's *t*-test.

Figure 3 | Global gene expression analysis on transduced neurons confirms the high specificity profile of the *Scn1a*-dCas9A system.

A, Schematic view of the experimental setting to perform gene expression profiling of Ctrl-dCas9A and *Scn1a*-dCas9A treated primary neurons. E17.5 embryo derived neurons were transduced with single lentiviruses (LV) at DIV 1 expressing either the Ctrl-dCas9A or *Scn1a*-dCas9A elements and processed for RNA extraction 48 h later (DIV 3). **B**, Volcano plots showing log10 p value as a function of log2 fold changes in gene expression in *Scn1a*-dCas9A treated neurons with respect to Ctrl-dCas9A. *Scn1a* is shown as a red dot; yellow dots represent off-target genes in the left panel and other *Scna* genes in the right panel; all other genes are shown as gray dots. **C**, RT-qPCRs for profiling expression of predicted off-targets (genes Prp4, BC024978, Olfr919 and Plrg1; left panel) or (**D)** other Scna genes (Scn2a, Scn3a, Scn4a, Scn5a, Scn7a, Scn8a, Scn9a, Scn11a; right panel). Plotted values are normalized on 18S rRNA and are expressed as relative to sgCtrl treated samples (value=1, not shown). n = 6; sg1p vs sgCtrl $p < 0.0004$, Student's *t*-test. Data are shown as mean ± s.e.m. with dots representing individual samples.

Figure 4 | *Scn1a*-dCasA increases neuronal excitability in cortical immature wild-type interneurons.

A, Schematic drawing showing the timeline of transduction with LV expressing the dCas9A systems on the primary wild-type GAD67-GFP neurons and their subsequent functional analysis. **B,** Representative images of a patch-clamp recorded interneuron expressing both GFP under the GAD67 promoter and tdTomato reflecting the active *Scn1a*-dCas9A system, scale bar 25 um. **C,** Representative current clamp traces of APs induced by a single current step in dCas9A (black trace, sgCtrl) or *Scn1a*-dCas9A interneurons (blue trace, sg1P). **D,** Firing frequency *vs* injected current for Ctrl- and *Scn1a*-dCas9A transduced interneurons (Ctrl-dCas9A n = 11; *Scn1a*-dCas9A n = 15). **E,** Histogram of the maximum frequency reached by interneurons during the current step protocol ($p = 0.03$, Mann-Whitney's *U*-test). **F,** Experimental design of activity clamp in primary neuronal cultures in the presence of 4AP (see Methods). **G,** Representative full traces and zoomed-in traces (**H**) for the activity clamp protocol in Ctrl- dCas9A (black trace, sgCtrl) and *Scn1a*-dCas9A (blue trace, sg1P) interneurons. **I,** Activity clamp analysis for the number of events during the full traces (left) and cumulative plot for APs frequency (right) (Ctrl- n = 10; *Scn1a*- dCas9A n = 12; $p = 0.0009$ unpaired Student`s *t*-test).

Figure 5 | *Scn1a*-dCas9A stimulates *Scn1a* basal expression and $Na_v1.1$ protein levels in *Scn1a*$^{+/-}$ hippocampal neurons.

A, Schematic drawing of the dCas9A treatments in E17.5 *Scn1a*$^{+/-}$ primary neurons. Neurons were transduced with either Ctrl-dCas9A or *Scn1a*-dCas9A system one day after plating and processed for RNA and protein extraction at 22-25 DIV**. B, C** RT-qPCRs for *Scn1a* transcriptional levels performed on RNA extracted from Ctrl-dCas9A or *Scn1a*-dCasA treated *Scn1a*$^{+/+}$(**B**) and *Scn1a*$^{+/-}$ (**C**) primary neurons. Plotted data are expressed as relative to Ctrl-dCas9A. *Scn1a*$^{+/+}$ n=18, p=0.068; *Scn1a*$^{+/-}$ n = 4, p < 0.0001, Student's *t*-test. **D**, Binary alignment map (BAM) within the mouse Scn1a transcript (NM_001313997.1). The red box depicts the region amplified and sequenced with high coverage. Ctrl-dCas9A and Scn1a-dCas9A variant allele frequency (VAF) tracks show the observed variant allele frequency. Ctrl-dCas9A and Scn1a-dCas9A read tracks display a sample of about 30 different sequencing reads per sample, where nucleotides diverging from the reference genome are highlighted. **E,** Western blot for $Na_V1.1$ and Calnexin on protein lysates from adult (P45) *Scn1a*$^{+/+}$ and *Scn1a*$^{+/-}$ mice (left panel) and from Ctrl-dCas9A and Scn1a-dCasA treated *Scn1a*$^{+/+}$ and *Scn1a*$^{+/-}$ neurons at 22-25 DIV (middle and right panel). **F**, Densitometric quantification of immunoreactive bands in the Western blots on adult mouse brains. Values corresponding to the $Na_V1.1$ band were normalized on Calnexin levels. (n = 3, p = 0.03, Student's *t*-test). **G,** Densitometric quantification of immunoreactive bands in the Western blots on *Scn1a*$^{+/+}$ and *Scn1a*$^{+/-}$ neurons transduced with Ctrl-and Scn1a-dCas9A.Values corresponding to the $Na_V1.1$ band were normalized on Calnexin levels, n=4 one-way Anova followed by Turkey's multiple comparisons test. Data are shown as mean ± s.e.m., with dots representing individual samples

Figure 6 | *Scn1a*-dCasA rescues neuronal excitability defects in cortical mature *Scn1a*$^{+/-}$ interneurons.

A, Schematic drawing showing the experimental timeframe for lentiviral transductions and functional analysis of *Scn1a*$^{+/+}$; GAD67-GFP$^+$ or *Scn1a*$^{+/-}$;GAD67-GFP$^+$ primary hippocampal neurons transduced with the two depicted lentiviruses. **B,** Representative images of a patch-clamp recorded *Scn1a*$^{+/-}$ interneuron expressing both GFP under the GAD67 promoter and tdTomato reflecting the active *Scn1a*-dCas9A system (see Methods). **C,D,** Representative current-clamp traces of APs induced by single current steps administered to Ctrl-dCas9A transduced WT interneurons (black trace), *Scn1a*-dCas9A transduced *Scn1a*$^{+/+}$interneurons (blue trace), Ctrl-dCas9A transduced *Scn1a*$^{+/-}$ interneurons (grey trace), *Scn1a*-dCas9A transduced *Scn1a*$^{+/-}$ interneurons (cyan trace). **E,F** Firing frequency *vs* injected current for Ctrl-dCas9A transduced (left panel) and *Scn1a*-dCas9A transduced (right panel) *Scn1a*$^{+/+}$ and *Scn1a*$^{+/-}$ interneurons. Ctrl-dCas9A

wild-type n = 12; Ctrl-dCas9A *Scn1a*$^{+/-}$ n = 10; *Scn1a*-dCas9A wild-type n = 10; *Scn1a*-dCas9A *Scn1a*$^{+/-}$ n=1 ($p < 0.05$; 2-way ANOVA). **G,H,** Histogram plots of the maximum frequency (**G**) and current threshold (**H**) reached by interneurons during the current step protocol ($p = 0.02$; $p = 0.04$; 2-way ANOVA/Bonferroni's multiple comparison tests). **I,J,** Activity-clamp analysis for the number of events during the full traces (**i**) and cumulative plot for AP frequency (**j**). ($p = 0.03$; 2-way ANOVA/Bonferroni's multiple comparison tests).

Figure 7 | *In vivo Scn1a*-dCas9A delivery through intracerebroventricular brain injections attenuates seizures in the *Scn1a*$^{+/-}$ mice.

A, Schematic illustration showing the experimental setting for the *in vivo* delivery of the *Scn1a*-dCas9A system through intracerebroventricular injections into P0 pups of AAVs (2.9) carrying the Ctrl-dCas9A and *Scn1a*-dCas9A system. After one week, treated mice were genotyped and *Scn1a*$^{+/-}$ animals were then selected for implantation of EEG electrodes and analysis of the epileptic phenotype. Wild-type (WT) litters were processed for molecular (2 weeks) and histological (5 weeks) characterization of the in vivo AAV targeting. Doxycicline (dox) was administered in drinking water or food until the final analysis. **B,** Scheme of cerebral cortex dissection in treated mice for Scn1a expression at mRNA level (Cx1: medial cortex; Cx2: lateral cortex; R: right; L: left). **C**, RT-qPCRs performed on dissected areas of the brains in Ctrl-dCas9A and *Scn1a*-dCas9A treated wild type mice (n = 6 for each group, $p = 0.042$ for Cx1_R and $p = 0.03$ for Cx1_L, Student's *t*-test). **D,** Mean (± s.e.m) threshold temperatures for the occurrence of myoclonic seizures (n = 6 for each group, $p = 0.048$, Student's *t*-test) and severity of the epileptic seizures evaluated by a modified Racine score (**E**) in Ctrl-dCas9A and *Scn1a*-dCas9A treated *Scn1a*$^{+/-}$ mice (n = 6 for each group, $p = 0.02$, Chi square test). Duration (**F**) and spike frequency (**G**) of temperature-induced seizures in Ctrl-dCas9A or *Scn1a*-dCas9A treated *Scn1a*$^{+/-}$ mice (n = 5 for Ctrl-dCas9A and n = 6 for Scn1a-dCas9A treated mice, $p = 0.029$ for duration and $p = 0.2$ for spike frequency, Student's *t*-test). **H**, Representative EEG traces of hyperthermia-induced seizures in Ctrl-dCas9A and *Scn1a*-dCas9A treated *Scn1a*$^{+/-}$ mice.

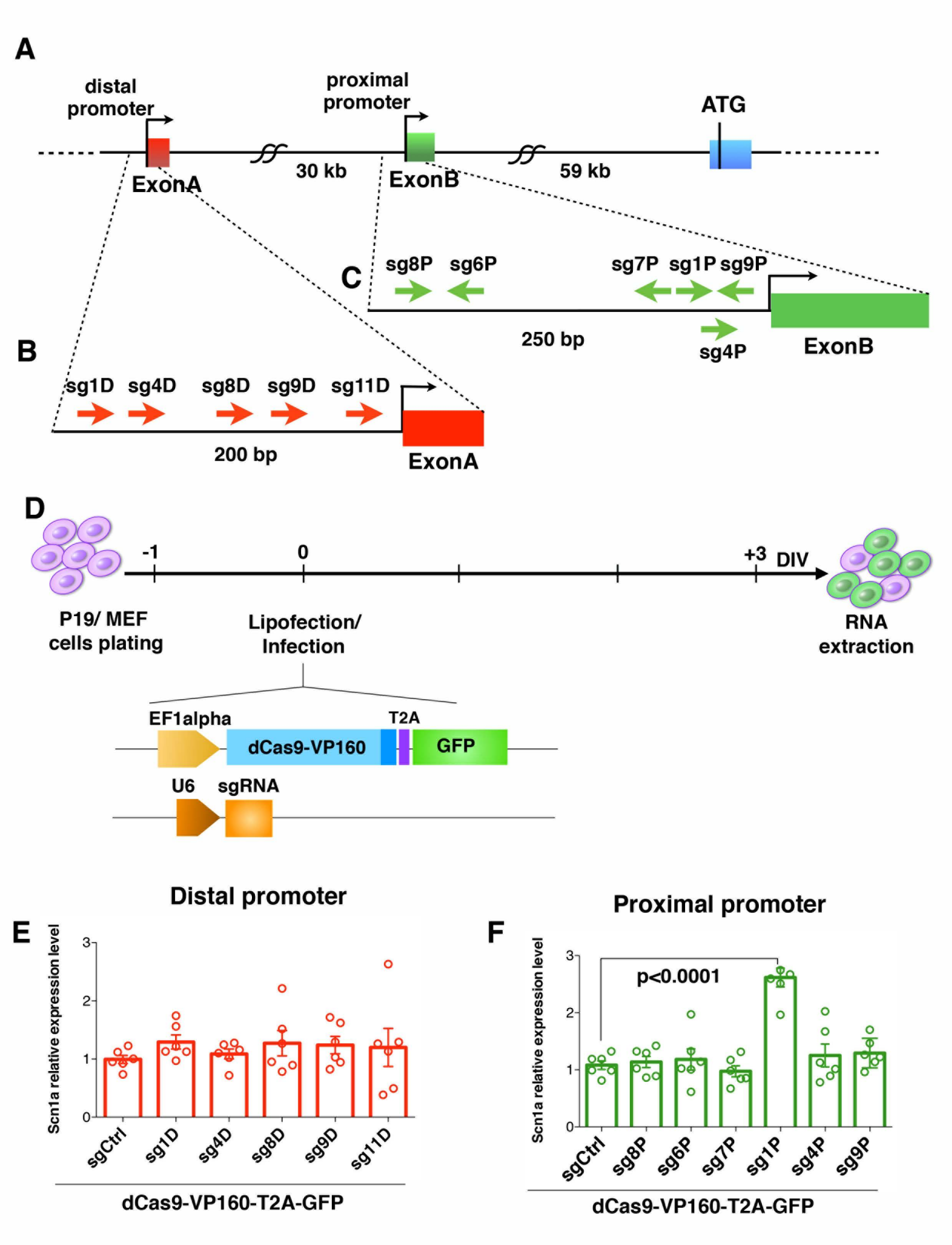
A
distal promoter
proximal promoter
ATG
ExonA
30 kb
ExonB
59 kb
B
sg1D sg4D sg8D sg9D sg11D
200 bp
ExonA
C
sg8P sg6P
sg7P sg1P sg9P
250 bp
sg4P
ExonB
D
-1
0
+3 DIV
P19/ MEF cells plating
Lipofection/ Infection
RNA extraction
EF1alpha
T2A
dCas9-VP160
GFP
U6
sgRNA
Distal promoter
E
Scn1a relative expression level
sgCtrl
sg1D
sg4D
sg8D
sg9D
sg11D
dCas9-VP160-T2A-GFP
Proximal promoter
F
p<0.0001
Scn1a relative expression level
sgCtrl
sg8P
sg6P
sg7P
sg1P
sg4P
sg9P
dCas9-VP160-T2A-GFP

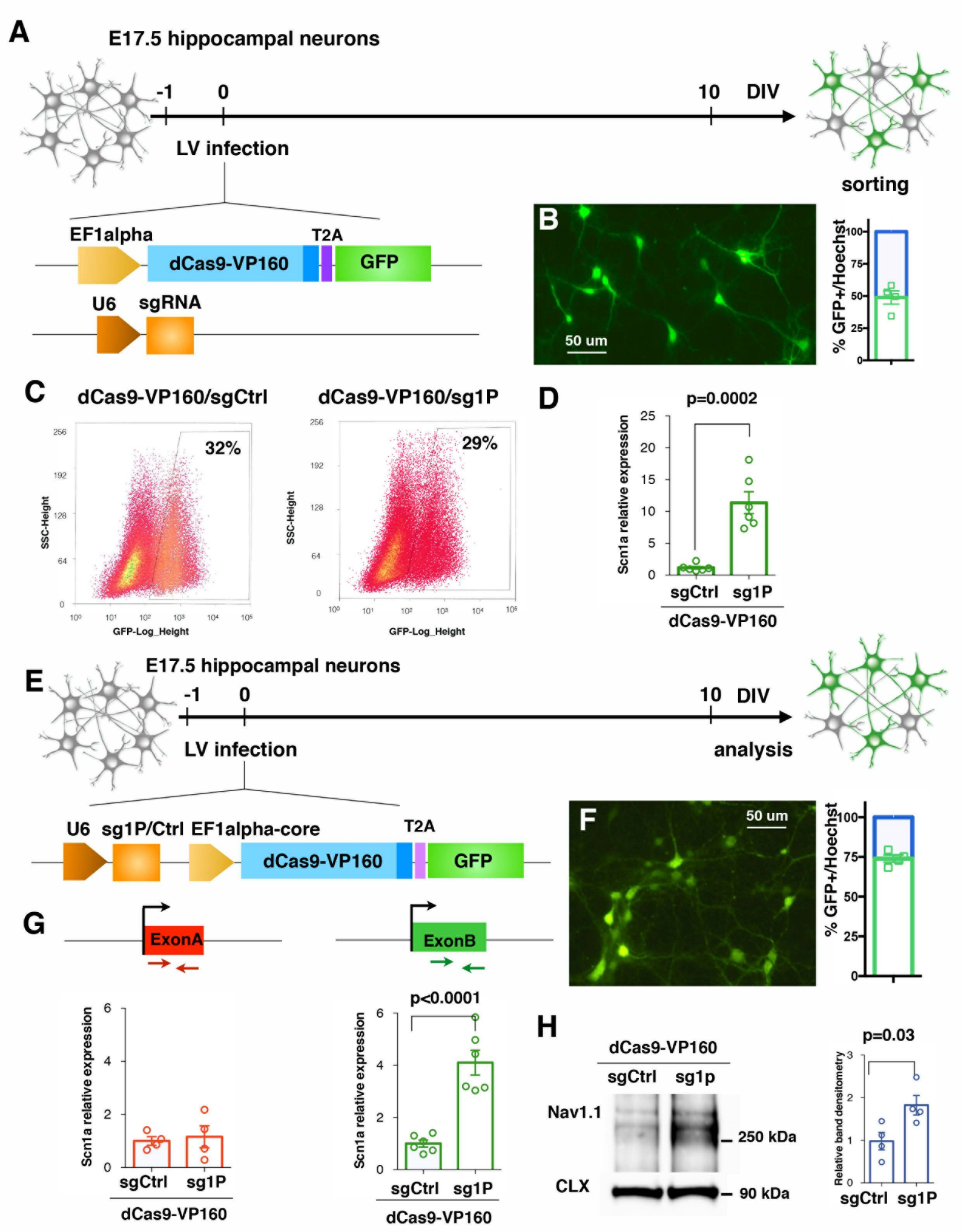
A
E17.5 hippocampal neurons
-1
0
10
DIV
LV infection
sorting
EF1alpha
T2A
dCas9-VP160
GFP
U6
sgRNA
B
50 um
% GFP+/Hoechst
C
dCas9-VP160/sgCtrl
dCas9-VP160/sg1P
32%
29%
SSC-Height
GFP-Log_Height
D
p=0.0002
Scn1a relative expression
sgCtrl
sg1P
dCas9-VP160
E
E17.5 hippocampal neurons
-1
0
10
DIV
LV infection
analysis
U6
sg1P/Ctrl
EF1alpha-core
T2A
dCas9-VP160
GFP
F
50 um
% GFP+/Hoechst
G
ExonA
ExonB
Scn1a relative expression
sgCtrl
sg1P
dCas9-VP160
p<0.0001
H
dCas9-VP160
sgCtrl
sg1p
Nav1.1
250 kDa
CLX
90 kDa
p=0.03
Relative band densitometry

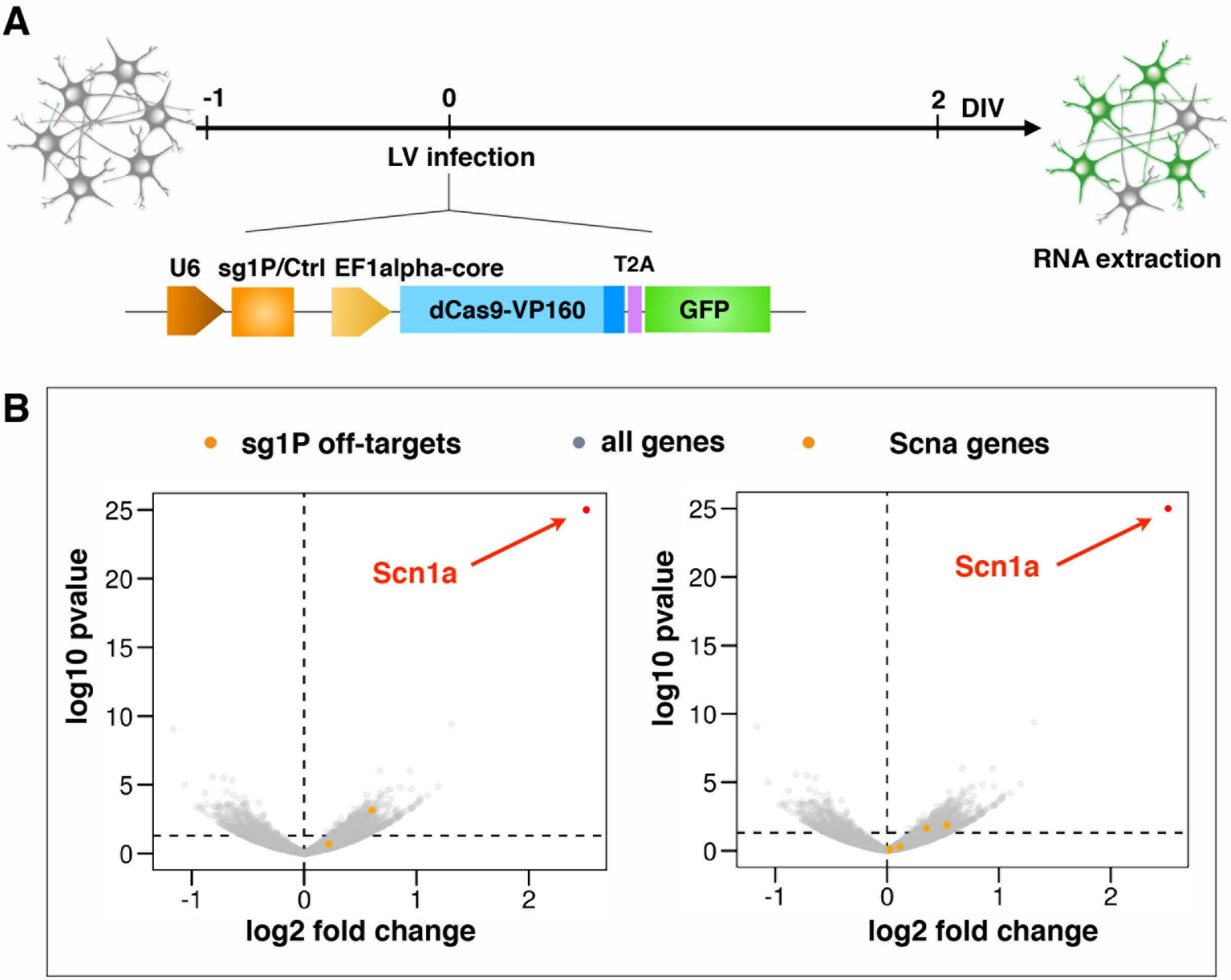
A
-1
0
2 DIV
LV infection
RNA extraction
U6
sg1P/Ctrl
EF1alpha-core
T2A
dCas9-VP160
GFP
B
sg1P off-targets
all genes
Scna genes
log10 pvalue
log2 fold change
Scn1a
Scn1a
C
Off-target gene expression
Scna gene expression
Relative expression level
Scn1a
Prp4
Bc024978
Olfr919
Plrg1
Relative expression level
Scn1a
Scn2a
Scn3a
Scn4a
Scn5a
Scn7a
Scn8a
Scn9a
Scn10a
Scn11a

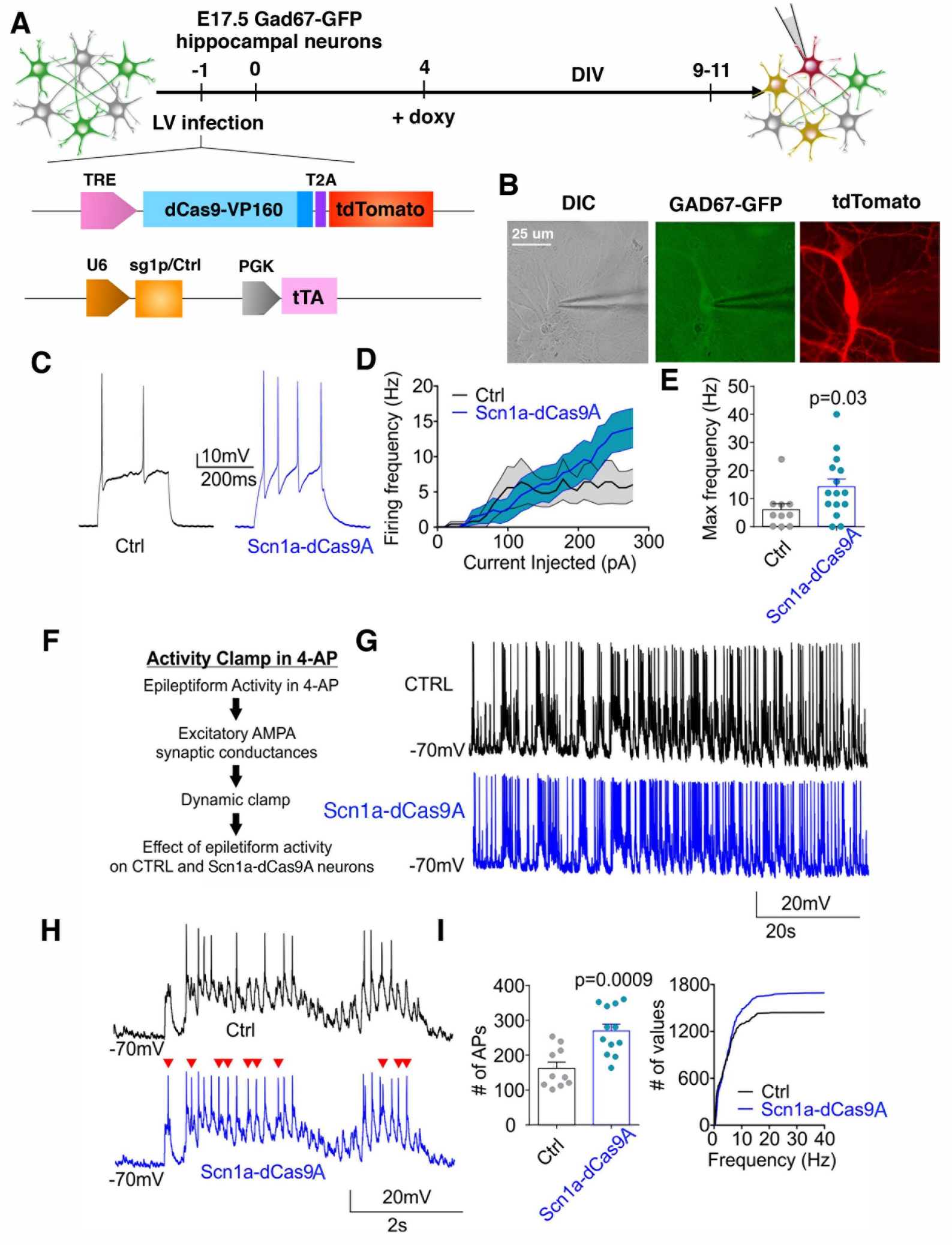
A
E17.5 Gad67-GFP
hippocampal neurons
-1
0
4
DIV
9-11
LV infection
+ doxy
TRE
dCas9-VP160
T2A
tdTomato
U6
sg1p/Ctrl
PGK
tTA
B
DIC
GAD67-GFP
tdTomato
25 um
C
10mV
200ms
Ctrl
Scn1a-dCas9A
D
Firing frequency (Hz)
Ctrl
Scn1a-dCas9A
Current Injected (pA)
E
Max frequency (Hz)
p=0.03
Ctrl
Scn1a-dCas9A
F
Activity Clamp in 4-AP
Epileptiform Activity in 4-AP
Excitatory AMPA
synaptic conductances
Dynamic clamp
Effect of epiletiform activity
on CTRL and Scn1a-dCas9A neurons
G
CTRL
-70mV
Scn1a-dCas9A
-70mV
20mV
20s
H
Ctrl
-70mV
-70mV
Scn1a-dCas9A
20mV
2s
I
p=0.0009
# of APs
Ctrl
Scn1a-dCas9A
# of values
Ctrl
Scn1a-dCas9A
Frequency (Hz)

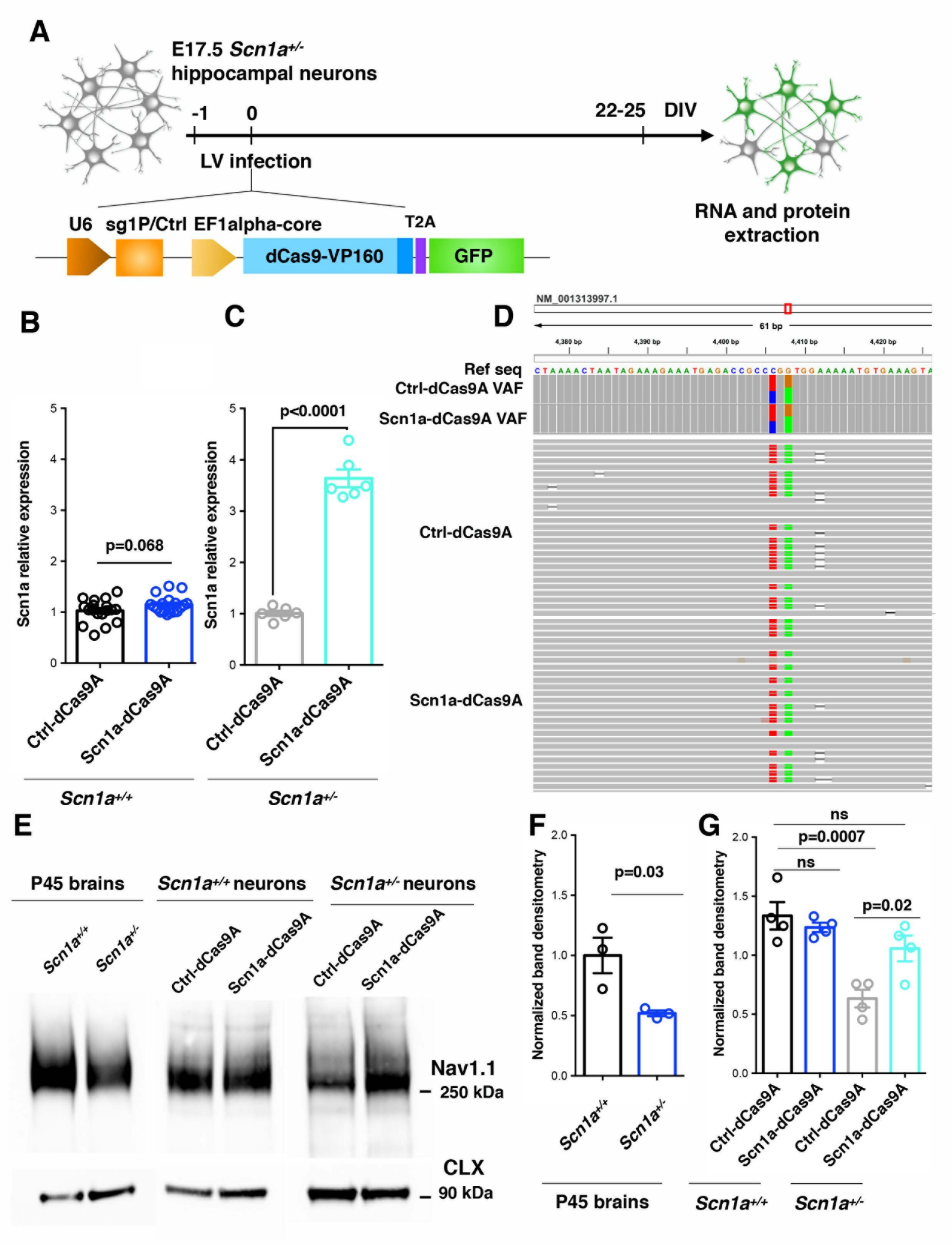
A
E17.5 Scn1a+/- hippocampal neurons
-1
0
22-25 DIV
LV infection
U6
sg1P/Ctrl
EF1alpha-core
T2A
dCas9-VP160
GFP
RNA and protein extraction
B
Scn1a relative expression
p=0.068
Ctrl-dCas9A
Scn1a-dCas9A
Scn1a+/+
C
Scn1a relative expression
p<0.0001
Ctrl-dCas9A
Scn1a-dCas9A
Scn1a+/-
D
NM_001313997.1
61 bp
4,380 bp
4,390 bp
4,400 bp
4,410 bp
4,420 bp
Ref seq
Ctrl-dCas9A VAF
Scn1a-dCas9A VAF
Ctrl-dCas9A
Scn1a-dCas9A
E
P45 brains
Scn1a+/- neurons
Scn1a+/+
Scn1a+/-
Ctrl-dCas9A
Scn1a-dCas9A
Nav1.1
250 kDa
CLX
90 kDa
F
Normalized band densitometry
p=0.03
Scn1a+/+
Scn1a+/-
P45 brains
G
Normalized band densitometry
ns
p=0.0007
ns
p=0.02
Ctrl-dCas9A
Scn1a-dCas9A
Ctrl-dCas9A
Scn1a-dCas9A
Scn1a+/+
Scn1a+/-

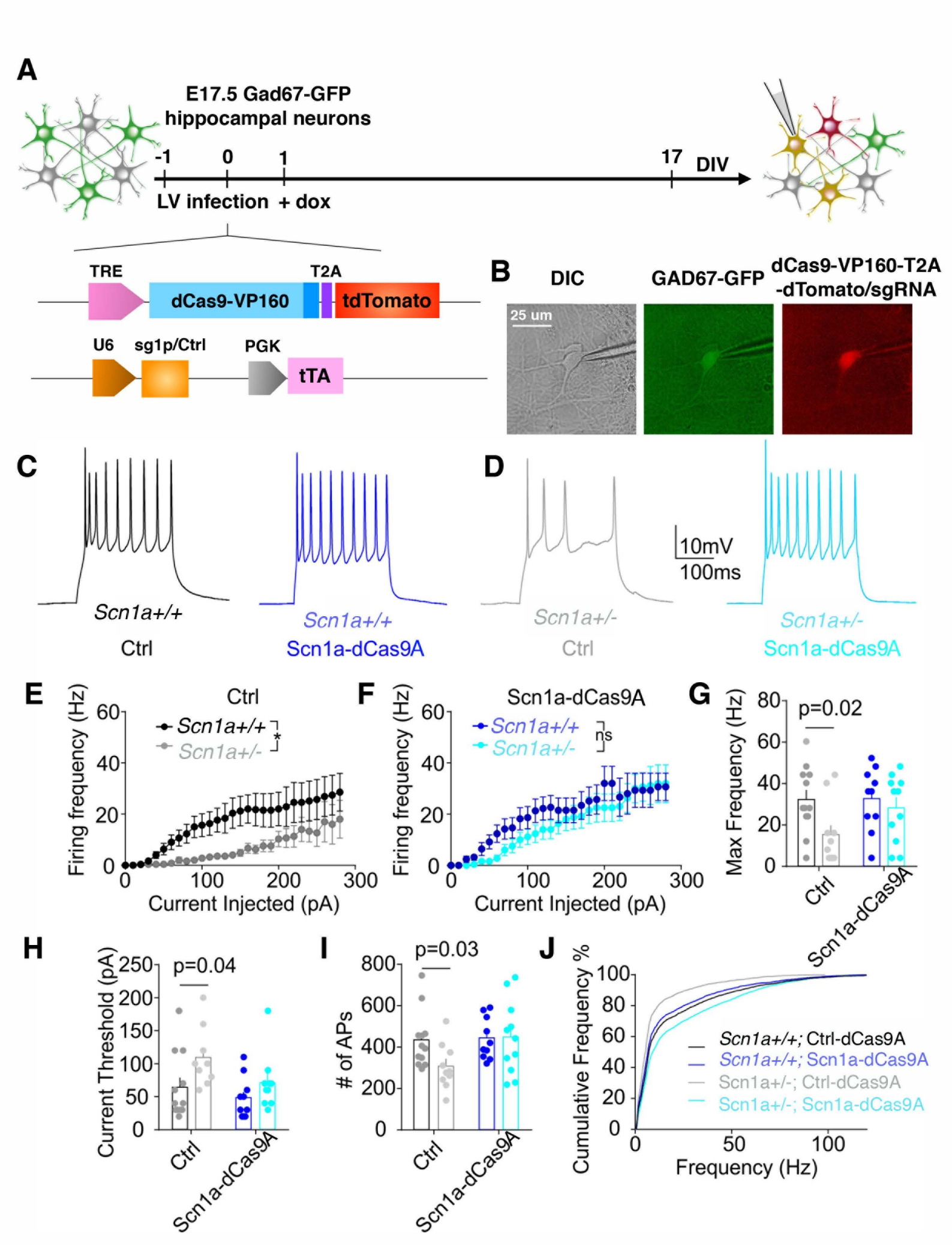
A
E17.5 Gad67-GFP
hippocampal neurons
-1
0
1
17
DIV
LV infection + dox
TRE
T2A
dCas9-VP160
tdTomato
U6
sg1p/Ctrl
PGK
tTA
B
DIC
GAD67-GFP
dCas9-VP160-T2A
-dTomato/sgRNA
25 um
C
Scn1a+/+
Ctrl
Scn1a+/+
Scn1a-dCas9A
D
10mV
100ms
Scn1a+/-
Ctrl
Scn1a+/-
Scn1a-dCas9A
E
Ctrl
Scn1a+/+
Scn1a+/-
*
Firing frequency (Hz)
Current Injected (pA)
F
Scn1a-dCas9A
Scn1a+/+
Scn1a+/-
ns
Firing frequency (Hz)
Current Injected (pA)
G
p=0.02
Max Frequency (Hz)
Ctrl
Scn1a-dCas9A
H
p=0.04
Current Threshold (pA)
Ctrl
Scn1a-dCas9A
I
p=0.03
# of APs
Ctrl
Scn1a-dCas9A
J
Cumulative Frequency %
Frequency (Hz)
Scn1a+/+; Ctrl-dCas9A
Scn1a+/+; Scn1a-dCas9A
Scn1a+/-; Ctrl-dCas9A
Scn1a+/-; Scn1a-dCas9A

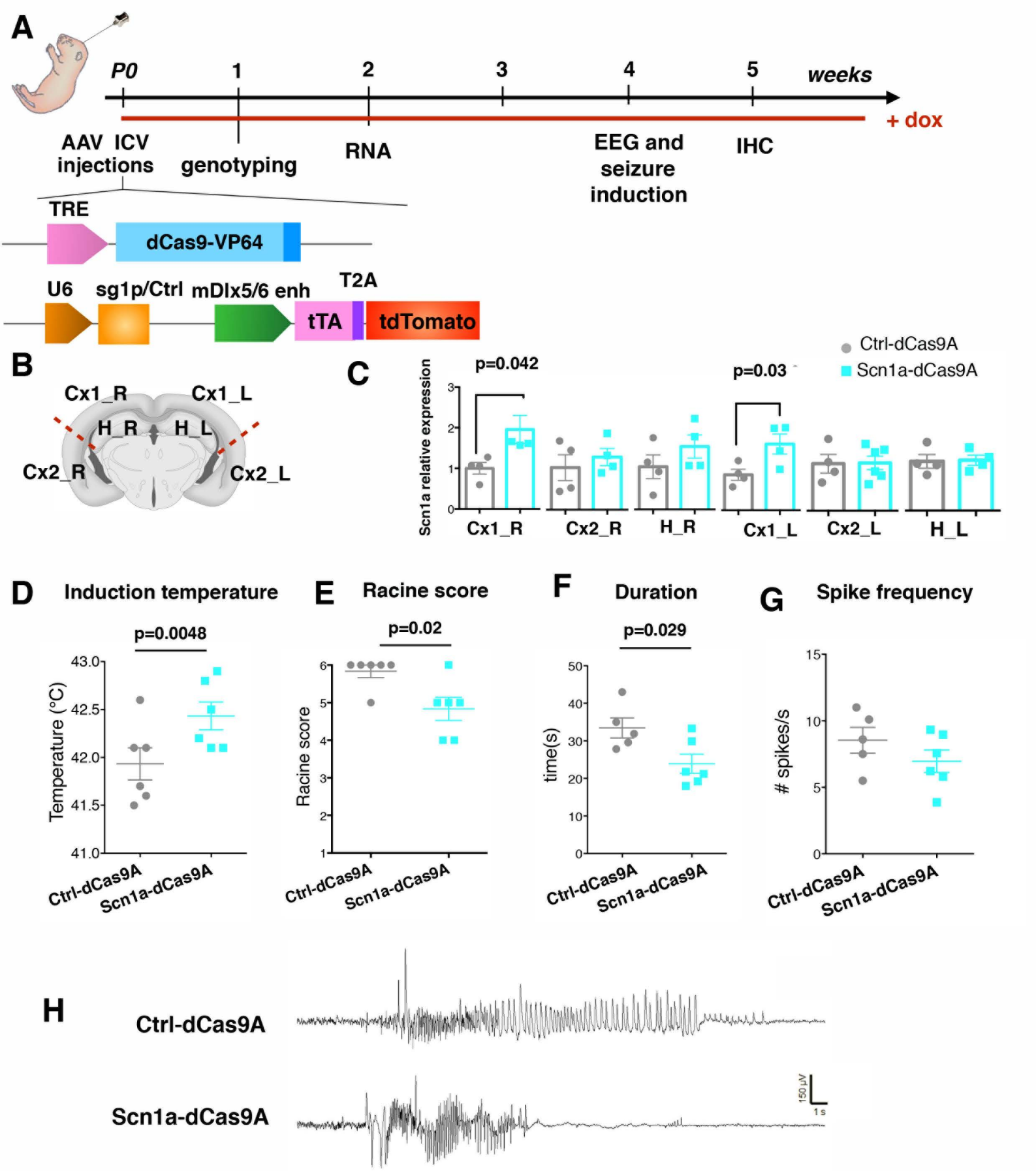
A
P0
1
2
3
4
5
weeks
+ dox
AAV ICV injections
genotyping
RNA
EEG and seizure induction
IHC
TRE
dCas9-VP64
U6
sg1p/Ctrl
mDlx5/6 enh
T2A
tTA
tdTomato
B
Cx1_R
Cx1_L
H_R
H_L
Cx2_R
Cx2_L
C
Ctrl-dCas9A
Scn1a-dCas9A
p=0.042
p=0.03
Scn1a relative expression
Cx1_R
Cx2_R
H_R
Cx1_L
Cx2_L
H_L
D
Induction temperature
p=0.0048
Temperature (°C)
Ctrl-dCas9A
Scn1a-dCas9A
E
Racine score
p=0.02
Racine score
F
Duration
p=0.029
time(s)
G
Spike frequency
spikes/s
H
Ctrl-dCas9A
Scn1a-dCas9A
150 µV
1 s

Figure S1. Related to Figure 1

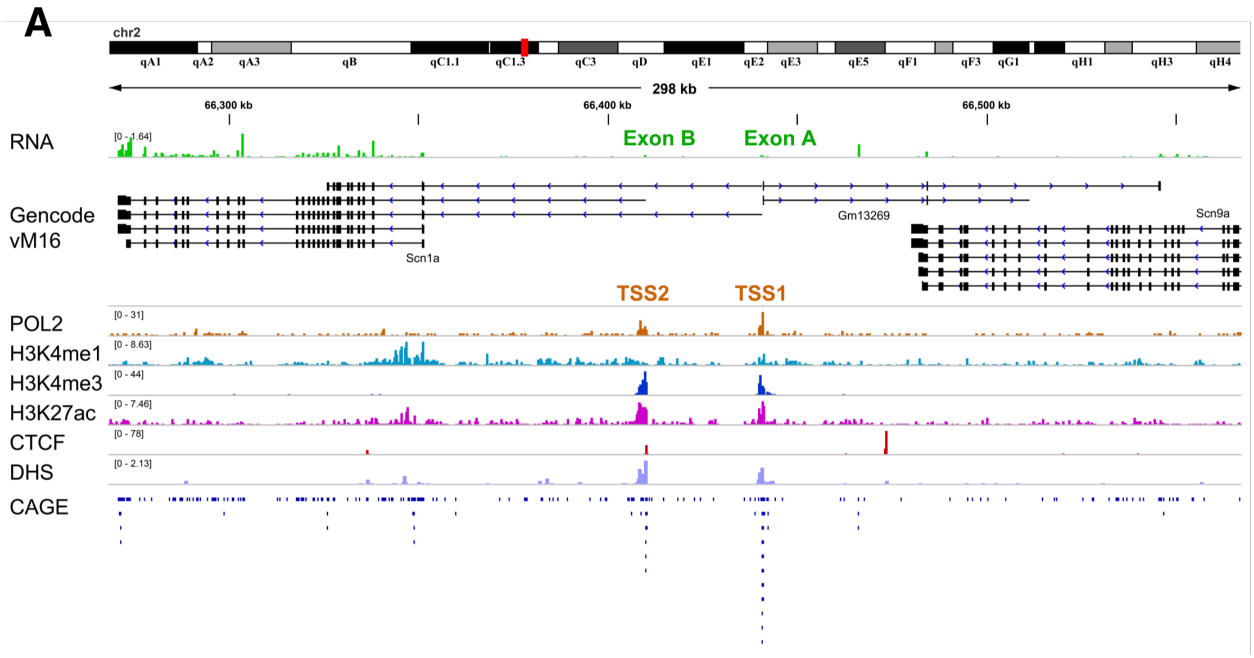

Figure S2. Related to Figure 1

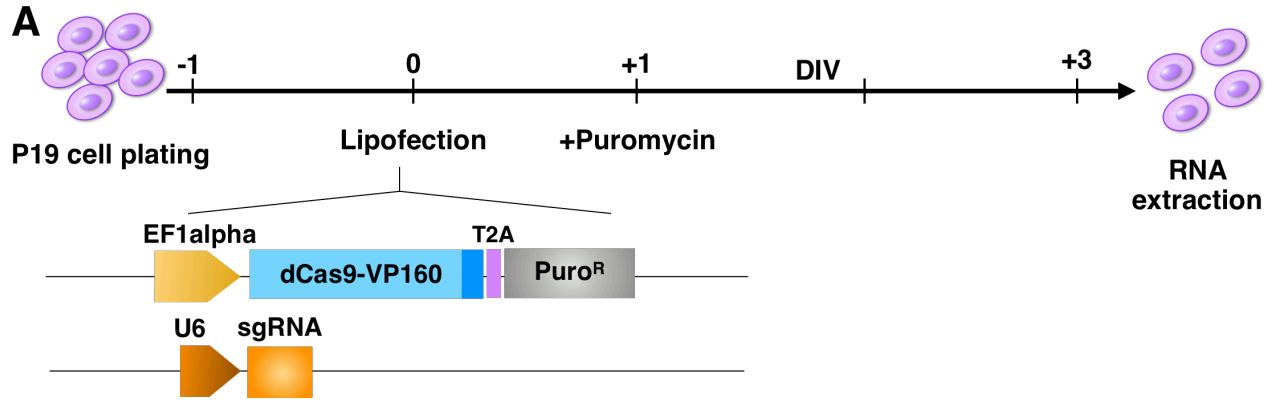

P19 cells

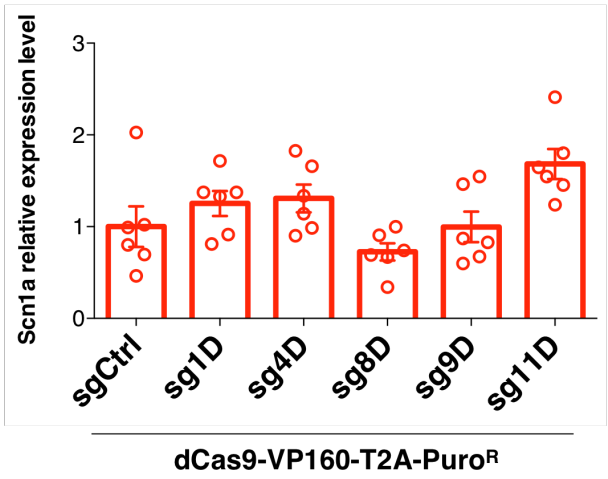

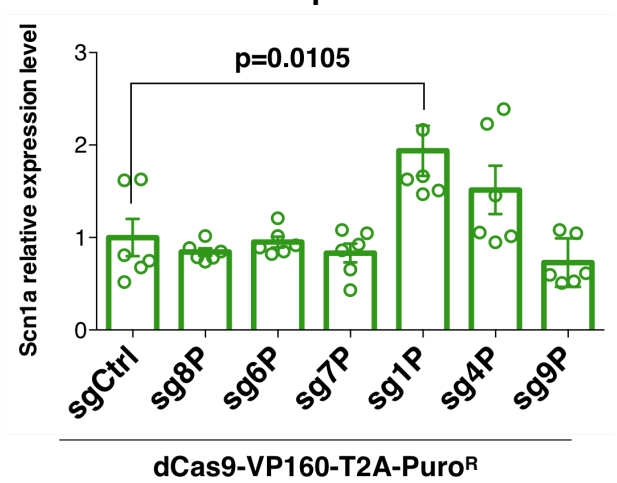

MEFs

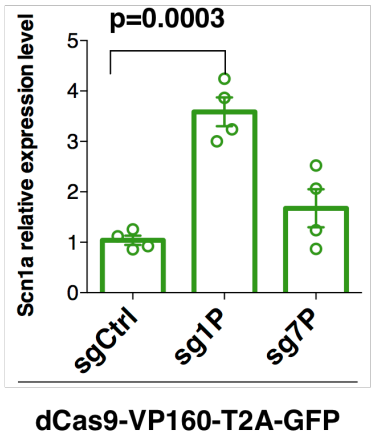

Figure S3. Related to Figure 4

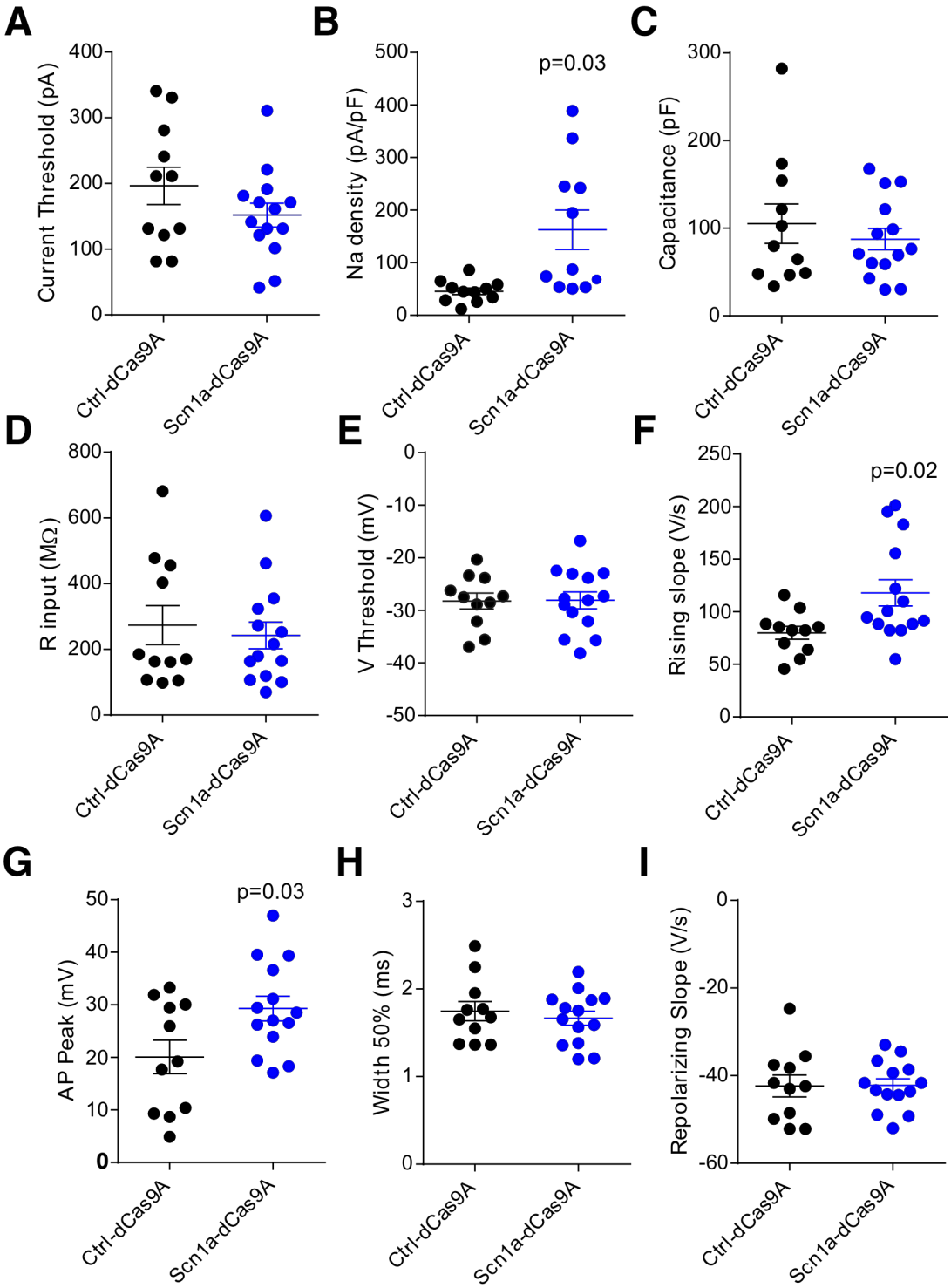

Figure S4. Related to Figure 4

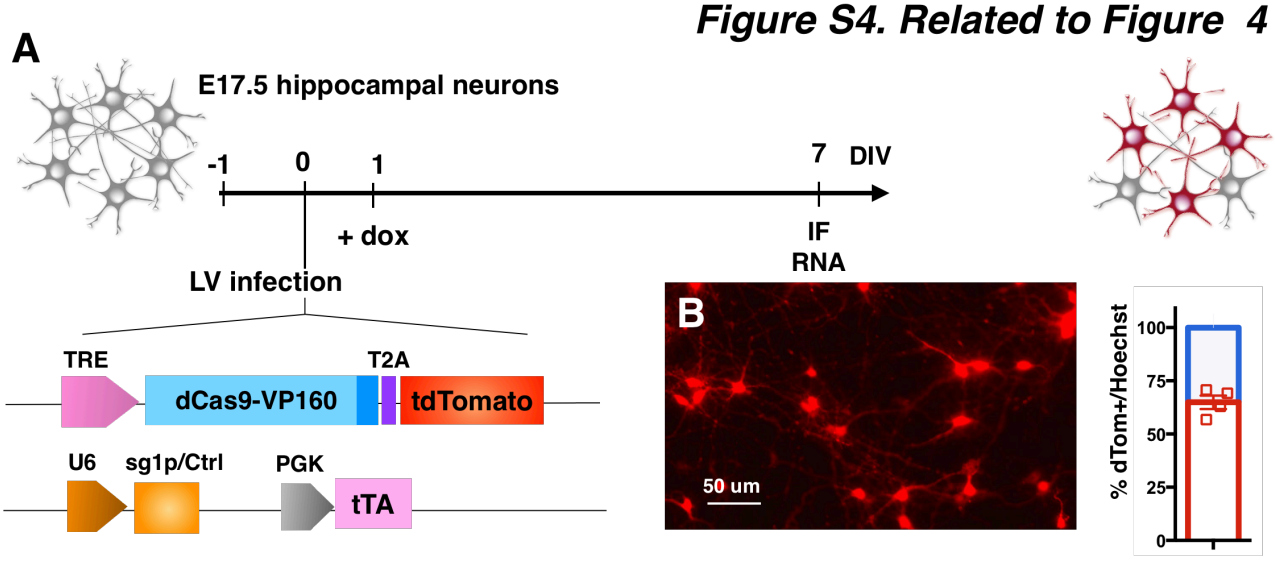

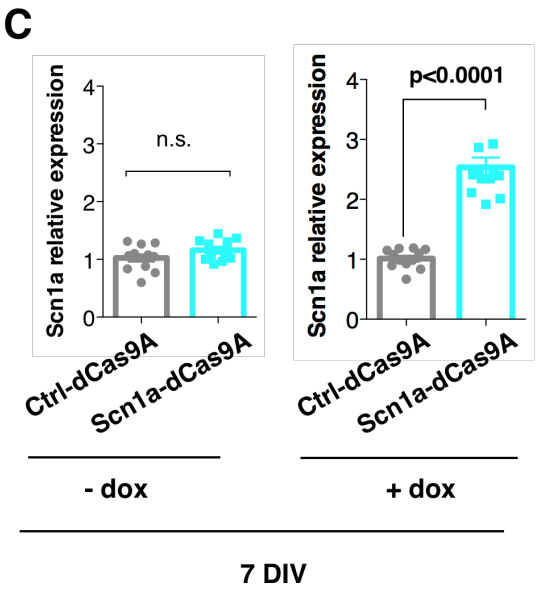

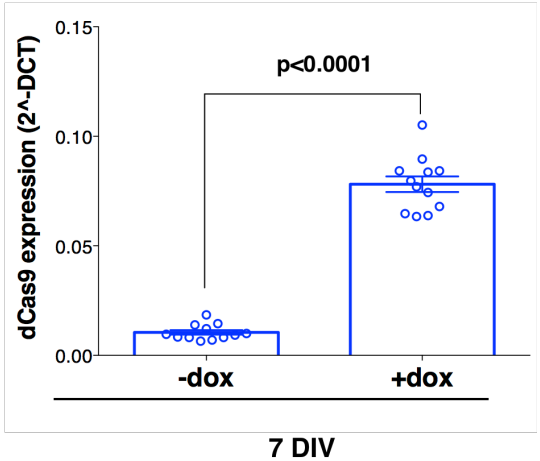

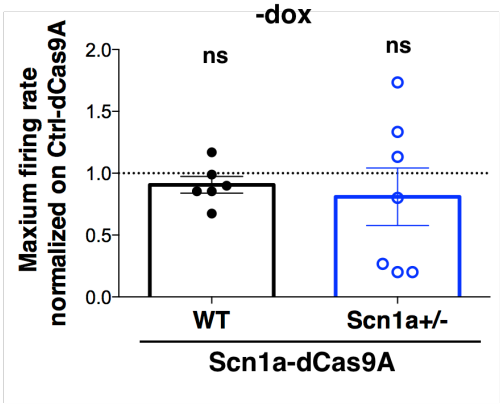

Figure S5. Related to Figure 6

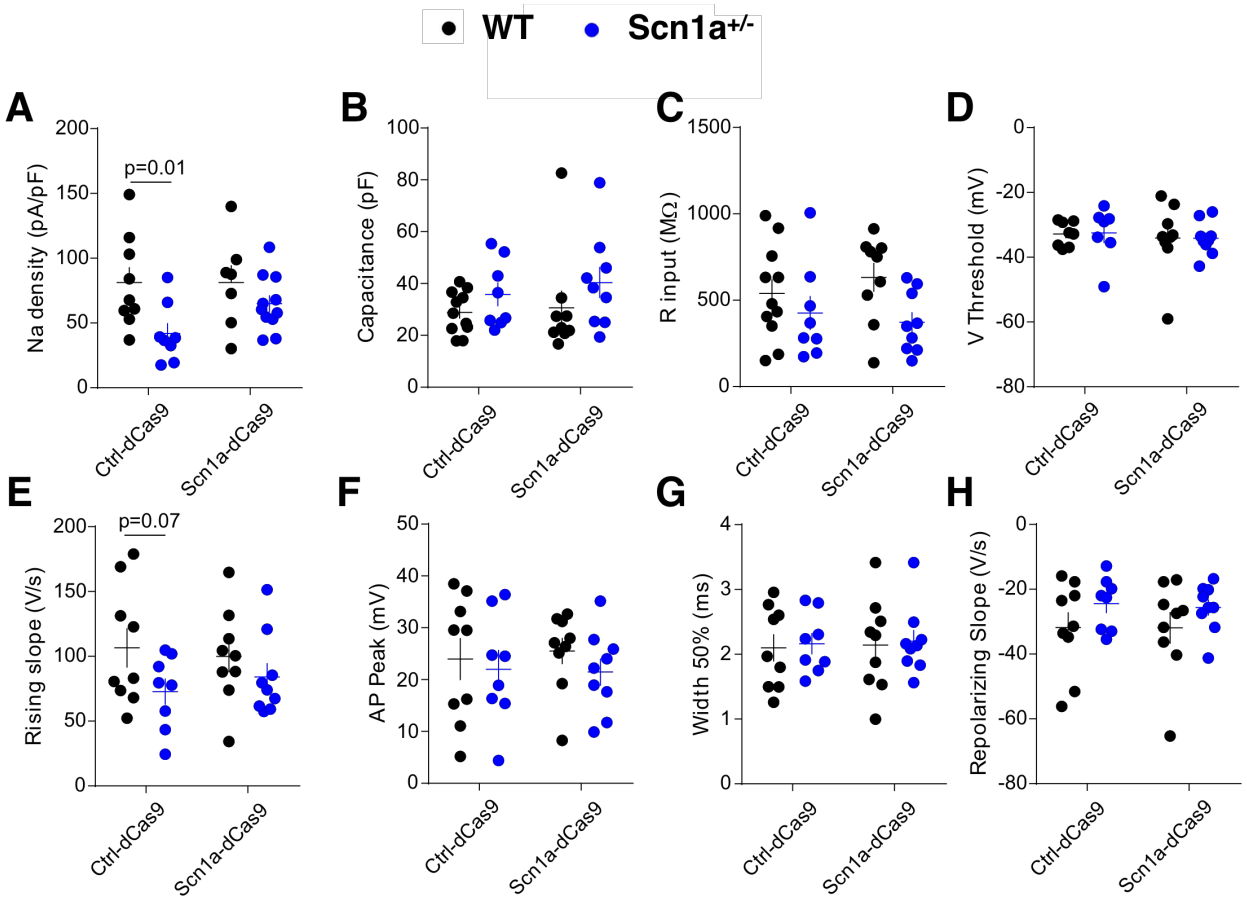

Figure S6. Related to Figure 7

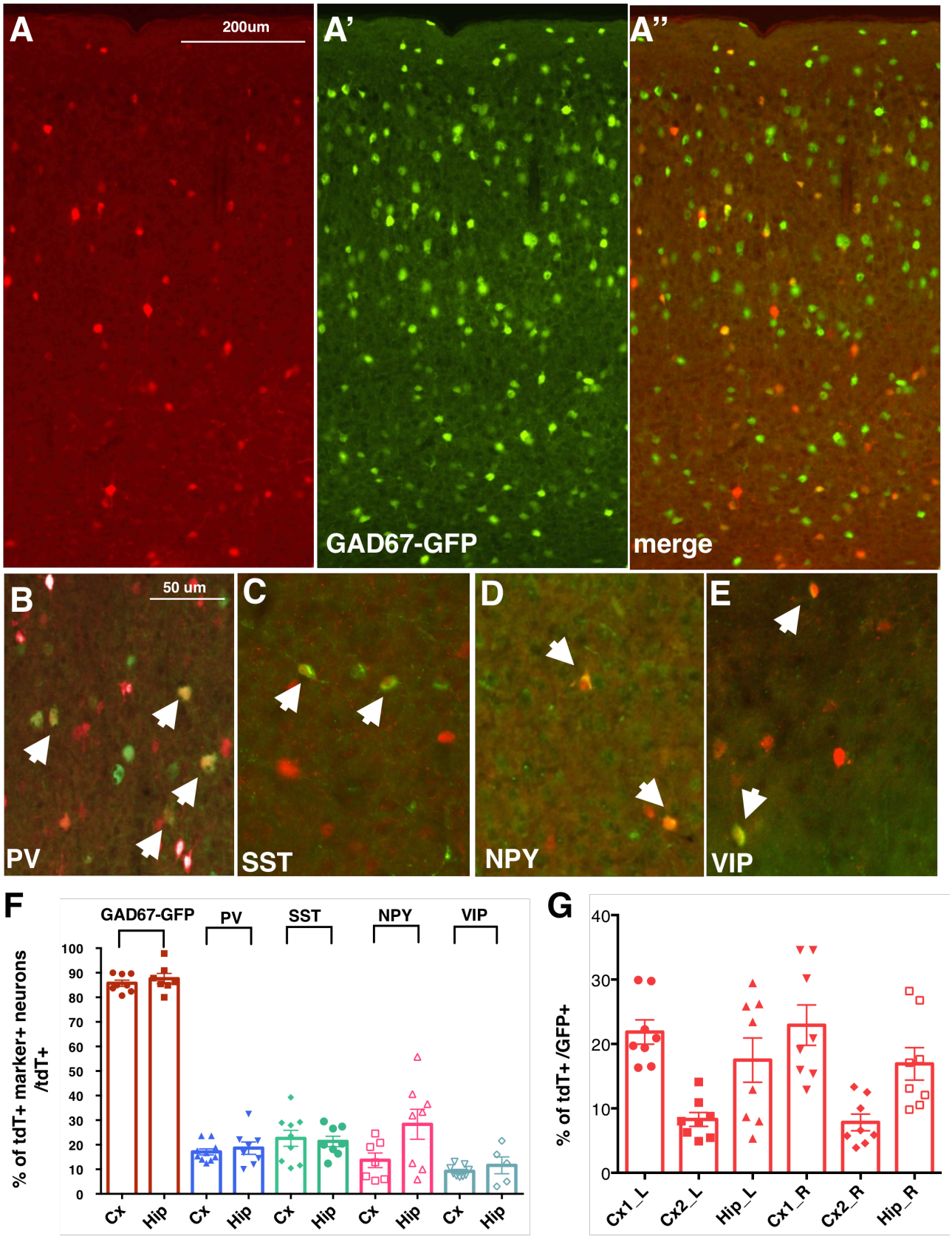

Figure S7. Related to Figure 7

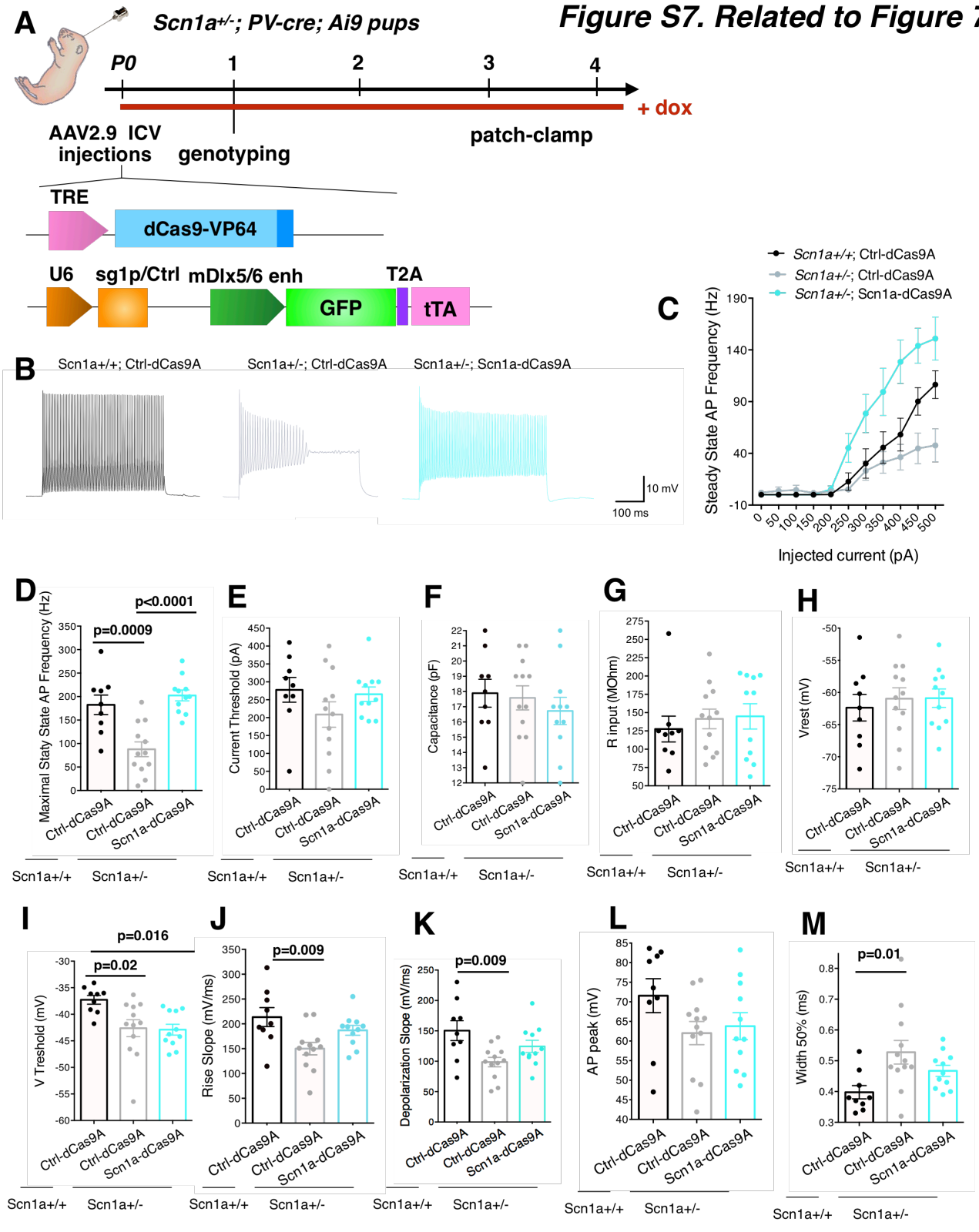

Figure S8. Related to Figure 7

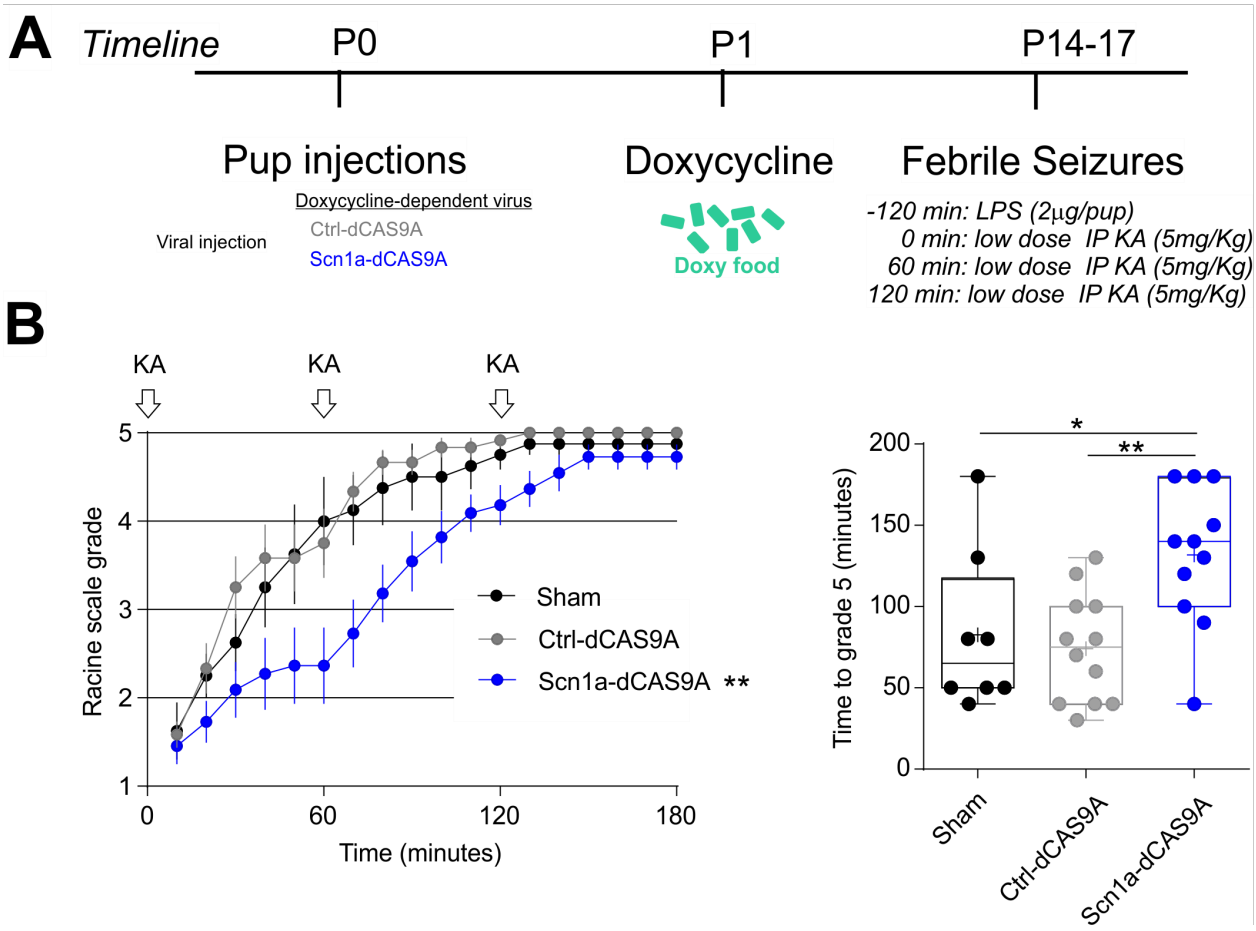

Table S1: Sequences of sgRNAs

sg1D	CGTTTTTGAAACGTTTTGGA AGG
sg4D	AGCATGAAAGCTAAATCTCC TGG
sg8D	ATAGGTCTCATTTTGTGGGT AGG
sg9D	TTGCATGGAAATCATGAACC AGG
sg11D	AAGTATTGGCAGCAGCAAGC AGG
sg8P	AATAAGCAAATTTCATTCAT GGG
sg6P	ATTGTTACTTTTACAGATTA CGG
sg7P	CCCCTTTGCTCTGCCTATCA TGG
sg1P	TAAGTCAATAGTTCCATGAT AGG
sg9P	CCCCTTTGCTCTGCCTATCA TGG
sg4P	CCATGATAGGCAGAGCAAAG TGG
sglacZ	TGCGAATACGCCCACGCGAT

Table S2: Primers for RT-qPCR

18s_F	GGTGAAATTCTTGGACCGGC
18s_R	GACTTTGGTTTCCCGGAAGC
Scn1a_F	CACCAACGCTTCCCTTGAGG
Scn1a_R	TGGACATTGGCCTGCATCAG
Scn1a_exA_F	GGTCCTGGTGGTACAAGCACT
Scn1a_exA_R	GAGGCTGCAGGAAGCTGAG
Scn2a_F	CCTCAGGAGGTCTATGCCAAA
Scn2a_R	GTGTCAGCTGGTTGCGAAAA
Scn3a_F	GCATTGCGTCCACGTAGATAA
Scn3a_R	GGAGCTGAAGACATGGGTCA
Scn4a_F	AGATCCCGCCTCCTGATTTA
Scn4a_R	ATCATGGGGGTGAGAGGAGT
Scn5a_F	TGGGAGAGGAGACAGTGTGG
Scn5a_R	CACGGGGATGATTGGACTTA
Scn7a_F	CCTTACCAACTTGCCTTGGA
Scn7a_R	ACCAACCAACCAACCAAACA
Scn8a_F	GCTTCTGCCATATCCCTCCA
Scn8a_R	GGCAGCTCCATCTTTCCATC
Scn9a_F	ATGGAAGATGCCAAGCAGTG
Scn9a_R	TGGATGTTTTGTGTGGCTCA
Scn10a_F	TCCCACCATCCTATGACAGC
Scn10a_R	ACTGAGGTCCAGGGCTCTTC
Scn11a_F	TTCATGGAGGCCAATCCTTT
Scn11a_R	TGACCTGCCTTTCAGCTTCA
Pde4b_F	TCAGCCAGGTCTAATCTGCCA
Prp4_F	GGTCCATGGTGACCTTCAAGA
Prp4_R	ATGTGGACTGTAGGTGGTGC
BC02_F	AGTGAGTGCAGGGGTCCT
BC02_R	GAAGGATGGTGGTTGGTGGG
Olfr919_F	CCTGGATGGTAGGTGGGGTA
Olfr919_R	GCAGGCAAGCTCCATCAATG
Plrg1_F	AGTTGCTACCGTGAGATGCC
Plrg1_R	TGGTTCGTCAGTGTCACTCG

Supplementary Figure Legends

Figure S1 | Bioinformatics analysis of the *Scn1a* gene locus for promoter regulatory region prediction.

Alignment to the *Scn1a* gene reference sequence of RNA-seq, ChIP-seqs, DNase-seq and CAGE- seq profiles related to adult mouse brains. The enrichment of markers associated with transcriptional activation in the regions upstream of the first two untranslated exons (Exon A and Exon B) of the gene highlights the presence of two TSS (TSS1 and TSS2) and allows to localize a distal promoter in the 200 bp upstream of exon-A and a proximal promoter upstream of the exon-B. POL2, RNA polymerase II ChIP-seq; H3K4me3, tri-methylation of lysine 4 on the histone H3 ChIP-seq; H3K4me1, mono- methylation of lysine 4 on histone H3 ChIP-seq; H3K27ac, acetylation of lysine 27 on histone H3 ChIP-seq; CTCF, factor that binds the CCCTC; DHS, DNase I Hyper Sensitivity mapping; CAGE-seq, Cap Analysis of Gene Expression-sequencing.

Figure S2 | Screening of sgRNAs for *Scn1a* gene activation by targeting its distal or proximal promoter in association with the dCas9-VP160-T2A-GFP in different cell types.

a, Screening of the guides lipofected in P19 cells in association with dCas9VP160-T2A-Puro^R. Quantitative RT-PCRs performed on RNA extracted from P19 cells 3 days after lipofection with dCas9VP160-T2A-Puro^R and sgRNAs targeting distal **(b)** or proximal **(c)** promoters to evaluate levels of *Scn1a* gene transcript. Data are normalized on 18S rRNA and relative to sgCtrl lipofected cells; n = 6, p = 0.0001, one-way ANOVA followed by Bonferroni multi comparison tests. **d**, RT-qPCR on RNA extracted from MEFs infected with sg1P and sg7P in association with dCas9VP160-T2A-Puro^R; n = 4, p = 0.0003, One-way ANOVA followed by Bonferroni's multiple comparison tests. Data are shown as mean ± s.e.m. with dots representing individual samples.

Figure S3 | The *Scn1a*-dCas9A system accelerates functional maturation of primary wild-type hippocampal neurons at 9-11 DIV.

Analysis of passive properties, voltage steps and current threshold (**a-d**), and single AP shape (**e-i**) in 9-11 DIV wild-type primary neurons transduced with either the Ctrl-dCas9A or *Scn1a*-dCas9A system. Student's *t* test was used for statistical analysis.

Figure S4 | Assessing the leakiness of the *Scn1a* gene activation by the *Scn1a*-dCas9A system.

A, Illustration of the dual LV doxycycline (dox) inducible system set for patch-clamp experiments *in vitro:* a first LV carrying dCas9-VP160 regulated by the rtTA responsive element (TRE) and a second

carrying the transactivator rtTA together with the sgRNA. Dox was administered or not at / DIV IF and RNA extraction were performed; **B**, anti-RFP immunofluorescence and quantification of tdTomato^{+} transduced cells over total neurons. **C**, Relative RT-qPCR for Scn1a performed on RNA extracted from either Ctrl-dCas9A or *Scn1a*-dCasA in WT neurons at 7 DIV in the absence or presence of dox. Data are expressed as ratios relative to Ctrl-dCas9A. **D,** RT-qPCR for dCas9 (2^-DCt) in neurons transduced with Scn1a-dCas9A system in the absence or presence of dox (n=12, $p<0.0001$ Student's *t* test. **E,** Histogram plot of maximum firing rate in Scn1a-dCas9A treated wt and Scn1a$^{+/-}$ GAD67-GFP neurons relative to Ctrl-dCas9A in the absence of dox (n=7, Student's *t* test).

Figure S5| The *Scn1a*-dCas9 system corrects some functional impairments in 18-20 DIV primary *Scn1a*$^{+/-}$ neurons while is not altering activity in corresponding wild-type neurons.
A-H, Analysis of passive properties, Na^{+} current density and single AP shape in *Scn1a*$^{+/+}$ (black dots) and *Scn1a*$^{+/-}$ (blue dots) primary neurons transduced with either the Ctrl-dCas9A or the *Scn1a*-dCas9A system.

Figure S6 | AAVs packaged with the Scn1a-dCas9A system controlled by the Dlx5/6 enhancer direct tdTomato expression specifically in cortical interneuron subpopulations *in vivo*.
A-A'', Anti-GFP and anti-RFP dual immunofluorescence in brain sections of P30 GAD67-GFP mice subjected to intracerebroventricular injections at P0 with AAVs carrying *Scn1a*-dCas9A elements, scale bars 200um. **B-E**, Representative cortical areas of P30 mouse brain sections transduced at P0 with the *Scn1a*- dCas9A elements stained for anti-PV, -SST, -NPY and -VIP in association with anti-RFP to reveal transduced neurons, scale bars 50 um. **F,** Quantification of the percentage of tdTomato^{+} cells co-expressing each of the interneuron markers listed above (GAD67-GFP, PV, SST, NPY and VIP) over the total number of tdTomato^{+} cells. **G**, Quantifications of the percentage of tdTomato^{+} cells over the total of GAD67-GFP+ cells in various areas (Cx1, Cx2 and Hip in each brain hemisphere). Data are shown as mean ± s.e.m., with dots representing individual quantifications.

Figure S7 | Scn1a-dCas9A treatment ameliorates firing in Scn1a+/- PV interneurons
A, Schematic illustration showing the experimental setting for ICV injections of Ctrl and Scn1a-dCas9A with GFP reporter into *Scn1a*$^{+/+}$ and *Scn1a*$^{+/-}$; PV-Cre Ai9 P0 pups. Transduced PV interneurons appear GFP^{+} and tdTomato^{+}. Dox was administered in drinking water until the final analysis. **B**, Representative traces recorded from GFP^{+}/tdTomato PV^{+} interneurons in somatosensory cortex (SSC) (P21-28). **C**, I/O plot analysis show impaired functionality in *Scn1a*$^{+/-}$ Ctrl-dCas9A compared to *Scn1a*$^{+/+}$; Ctrl-dCas9A interneurons which is recovered in *Scn1a*$^{+/-}$;Scn1a-dCas9A PV

interneurons (p=0.003, two-way ANOVA/Bonferroni). **D.** Maximal steady state AP frequency and other passive and AP parameters of *Scn1a*$^{+/+}$; Ctrl-dCas9A and *Scn1a*$^{+/-}$; Ctrl-/ Scn1a-dCas9A transduced PV interneurons (one-way ANOVA/Bonferroni's multiple comparison tests).

Figure S8 | Upregulation of Nav1.1 during early development is protective against febrile seizures. A. Timeline of the experimental plan. **B.** *Left.* Racine scale scoring following low dose KA injections every hour over a 3-hour experimental time period with behavioural scoring every 10 minutes. ** $p<0.01$, two-way ANOVA, Sham or Ctrl-dCAS9A vs Scn1a-dCAS9A. *Right.* Box plots of the time taken to reach grade 5. Middle line represents the median, "+" the mean and the box, the 10-90 percentile range. *$p<0.05$, **$p<0.01$, one-way ANOVA followed by Bonferroni multi-comparison test.

Supplementary Table 1: Sequences of sgRNAs.

Supplementary Table 2: Primers for RT-qPCRs.